



HAL
open science

A NONISOTHERMAL THERMODYNAMICAL MODEL OF LIQUID-VAPOR INTERACTION WITH METASTABILITY

Hala Ghazi, Francois James, H el ene Mathis

► **To cite this version:**

Hala Ghazi, Francois James, H el ene Mathis. A NONISOTHERMAL THERMODYNAMICAL MODEL OF LIQUID-VAPOR INTERACTION WITH METASTABILITY. *Discrete and Continuous Dynamical Systems - Series B*, 2021, 26 (5), pp.2371–2409. 10.3934/dcdsb.2020183 . hal-02336478v2

HAL Id: hal-02336478

<https://hal.science/hal-02336478v2>

Submitted on 2 Jun 2021

HAL is a multi-disciplinary open access archive for the deposit and dissemination of scientific research documents, whether they are published or not. The documents may come from teaching and research institutions in France or abroad, or from public or private research centers.

L'archive ouverte pluridisciplinaire **HAL**, est destin ee au d ep ot et  a la diffusion de documents scientifiques de niveau recherche, publi es ou non,  emanant des  tablissements d'enseignement et de recherche franais ou  trangers, des laboratoires publics ou priv es.

1 may make the liquid water being metastable: its temperature increases above the
 2 saturation temperature; the water is then called superheated. The metastability
 3 corresponds then to a delay in vaporization. Even a small perturbation of the
 4 metastable water may lead to the brutal appearance of a vaporization wave. In
 5 [4] an analogous phenomenon is highlighted. Liquid water can be brought to a su-
 6 perheated state by means of a very rapid depressurization. The depressurization is
 7 stopped suddenly by an explosive nucleation causing, in its turn, an increase of the
 8 pressure.

9 As pointed out in [7], such compressible two-phase flows are characterized by
 10 three main difficulties. The first two difficulties are linked to the dynamics of the
 11 fluid, namely the compressibility of both phases and the presence of the moving
 12 interface between them. The third difficulty lies in the modelling of the thermody-
 13 namical exchanges which occur at the interface. The references [31] and [35] focus on
 14 the two first difficulties and propose models coming from the Bear-Nunziato model
 15 for compressible two-phase flows. The models are either 6 or 5 equations models,
 16 possibly including pressure and velocity interfacial terms. Each phase possesses his
 17 own convex Equation of State (EoS), namely a stiffened gas law (or a Mie-Grüneisen
 18 generalization). Relaxation towards thermodynamical equilibrium is assumed to be
 19 infinitely fast, so that metastable states appear far from the vaporization fronts. In
 20 [7, 8] and [9], the authors improve this approach by using the realistic tabulated
 21 law IAPWS-IF97 EoS coupled with cubic interpolation and accurate HLLC-type
 22 numerical scheme. They compare different models of a same hierarchy. Starting
 23 from a single-velocity six equations model with full disequilibrium, they consider
 24 a homogeneous equilibrium model where the liquid and the vapor are at thermo-
 25 dynamical equilibrium (meaning stable) and a homogeneous relaxation model in
 26 which the liquid is assumed to be metastable and the vapor is at saturation. Again
 27 emphasis is given to the two first difficulties of compressible two-phase flows, the
 28 question of metastability being addressed solely in the choice of the complex EoS.

29 In the present paper, we focus on the third difficulty, namely the modelling
 30 of thermodynamical transfers and the appearance of metastable states. As the
 31 dynamics of the flow is concerned, we adopt the strategy proposed in [7, 8] and
 32 consider the homogeneous relaxation model given in [18] and [22]. We assume that
 33 the two phases evolve with the same velocity and consider the mass, momentum
 34 and energy conservation equation of the flow. The specificity is to assume that
 35 the two phases follow the same non-convex EoS, namely a reduced form of the van
 36 der Waals equation. Because the model involves a mixture pressure based on this
 37 cubic equation, the convective system is not strictly hyperbolic, notably in the van
 38 der Waals spinodal zone. To get rid of this problem, the pressure is relaxed and
 39 depends on additional quantities, which are the fractions of volume, mass and energy
 40 of one of the phases. These fractions obey to convective equations with relaxation
 41 terms towards the thermodynamic equilibrium. The core of the paper is the proper
 42 definition of these relaxation terms. To do so, we extend the method we proposed
 43 in [24] in the isothermal case and provide a characterization of thermodynamic
 44 equilibria which are either saturation states, stable and metastable states.

45 In a first section, we recall some basic facts of thermodynamics in the extensive
 46 and intensive form [5], notably the notion of entropy. We focus on the van der Waals
 47 model, which is well-known to depict stable and metastable states but is classically
 48 used with a convexification correction to properly depict saturation. It turns out
 49 that the representation of metastable states of the van der Waals model is done in

1 the volume-pressure plane, although the equations of motion require to manipulate
 2 phase diagram and EoS defined in the volume-energy plane. A large part of Section
 3 2.2 then concerns the representation of stable, metastable and spinodal zone in the
 4 volume-energy plane.

5 In Section 3 we investigate the thermodynamic stability of a system described
 6 by the non convex EoS of van der Waals in its reduced form. As suggested in [5,
 7 chap. 8], introducing heterogeneity in a system is the hallmark of phase transition.
 8 Hence, in order to introduce heterogeneity in the system, we decompose it in an
 9 arbitrary number of subsystems depicted by the same nonconvex EoS. The second
 10 principle of thermodynamics leads to a constrained maximization problem on the
 11 mixture entropy. It turns out that the number of subsystems is limited to two,
 12 in accordance with the Gibbs phase rule. Then the study of the optimization
 13 problem leads to two possible kinds of maximizers, either saturation states or states
 14 corresponding to the identification of the two phases. In the latter case, there
 15 is no distinction between the two phases and all the states belonging to the van
 16 der Waals EoS are possible maximizers, including the non-admissible (physically
 17 unstable) states of the spinodal zone. On the other hand, the saturation states
 18 correspond to the coexistence of the two phases at saturation, with equality of the
 19 pressures, temperatures and chemical potentials of the two phases, corresponding
 20 to the convexification of the EoS.

21 Section 4 provides a dynamical description of the thermodynamic equilibrium
 22 and of its two kinds of equilibrium states. Following the approach developed in [24]
 23 and [15] in the isothermal case, we introduce a dynamical system whose long-time
 24 equilibria coincide with the maxima of the above optimization problem, under a
 25 mixture entropy growth criterion. We focus in this paper on a dynamical system on
 26 the fractions of volume, mass and energy of the phase 1. The system is designed to
 27 recover the above two possible equilibria: either saturation states or states corre-
 28 sponding to the identification of the two phases. In the latter case, the equilibrium
 29 is characterized by the equality of all the fractions which converge asymptotically
 30 to some value belonging to $]0, 1[$. Hence, as the two phases identify, the fractions
 31 are not equal to 0 or 1, in contrast with the Baer-Nunziato type two-phase models
 32 [1]. This is one fundamental feature of the dynamical model we propose. Another
 33 property stands in the attractivity of the equilibria and their attraction basins. If
 34 the energy-volume state of the mixture belongs to the spinodal zone, then the cor-
 35 responding equilibrium is a saturation state, whatever the initial conditions of the
 36 dynamical system are. Thus the dynamical system gets rid of unstable states of
 37 the spinodal zone by construction. On the other hand, if the mixture state belongs
 38 to a metastable zone, there are two possible equilibria depending on the perturba-
 39 tion: either the identification of the two phases to the mixture metastable state or
 40 a saturation state. This interesting property was already highlighted in [24, 15] and
 41 is extended here to the non-isothermal case. Numerical simulations illustrate the
 42 attraction of each equilibria and typical trajectories of the dynamical system in the
 43 volume-energy plane, volume-pressure plane and in the fractions domain.

44 Finally, Section 5 addresses the coupling between the thermodynamics and the
 45 compressible dynamics of the two-phase flows we are interested in. Following the
 46 approach in [18, 22, 7], we consider that the fluid is homogeneous in the sense that
 47 the two phases evolve with the same velocity. Then the model is based on the
 48 conservation equations of total mass, momentum and energy. To close the system,
 49 it is endowed with a complex equation of state depending on the fractions of volume,

1 mass and energy of one of the phases. To ensure the return to the thermodynamic
 2 equilibrium, the evolution equations of the fractions admit relaxation source terms
 3 derived from the dynamical system studied in Section 4. Because the mixture
 4 pressure involves the van der Waals EoS, the hyperbolicity is non strict. However,
 5 it has been proved in [24] that the domains of hyperbolicity of the complete model
 6 strongly depend on the attraction basins of the dynamical system. In order to
 7 illustrate the dynamical behaviour of the model, we use a simple numerical scheme
 8 based on a fractional step approach: the convective part is approximated by an
 9 explicit HLLC solver while the source terms is integrated by a RK4 method.

10 2. THERMODYNAMIC ASSUMPTIONS AND THE VAN DER WAALS EOS

11 **2.1. Description of a single fluid.** We consider a monocomponent fluid of mass
 12 $M \geq 0$, occupying a volume $V \geq 0$ with internal energy $E \geq 0$. Following the Gibbs
 13 formalism [16, 5], we introduce the extensive entropy S of the fluid as a function of
 14 its mass M , volume V and energy E :

$$(1) \quad S : (M, V, E) \mapsto S(M, V, E).$$

15 All the above quantities are said extensive, in the sense that if the system is doubled,
 16 then its mass, volume, energy and entropy are doubled as well. Any extensive
 17 quantity $\Phi : E \subset \mathbb{R}^n \rightarrow \mathbb{R}$ is said positively homogeneous of degree 1 (PH1), and
 18 satisfies

$$(2) \quad \forall \lambda > 0, \forall x \in E \quad \Phi(\lambda x) = \lambda \Phi(x).$$

19 Especially for the entropy function S , the PH1 property (2) reads

$$(3) \quad \forall \lambda > 0, \quad S(\lambda M, \lambda V, \lambda E) = \lambda S(M, V, E).$$

20 We assume that the entropy function S belongs to $C^2(\mathbb{R}^+ \times \mathbb{R}^+ \times \mathbb{R}^+)$. It allows to
 21 introduce intensive quantities, that are positively homogeneous functions of degree
 22 0 (PH0), corresponding to derivatives of extensive functions. From the gradient
 23 vector ∇S of the entropy S , we commonly define the pressure p , the temperature
 24 T and the chemical potential μ by

$$(4) \quad \frac{1}{T} = \frac{\partial S}{\partial E}(M, V, E), \quad \frac{p}{T} = \frac{\partial S}{\partial V}(M, V, E), \quad \frac{\mu}{T} = -\frac{\partial S}{\partial M}(M, V, E),$$

25 leading to the fundamental thermodynamics extensive Gibbs relation

$$(5) \quad dS = -\frac{\mu}{T}dM + \frac{p}{T}dV + \frac{1}{T}dE.$$

26 Standard thermodynamics requires that

$$(6) \quad T = \left(\frac{\partial S}{\partial E} \right)^{-1} > 0.$$

27 Since the entropy S is a PH1 function, it verifies the Euler relation

$$(7) \quad S(M, V, E) = \nabla S(M, V, E) \cdot \begin{pmatrix} M \\ V \\ E \end{pmatrix},$$

28 which, combined with the definitions (4), gives

$$(8) \quad S(M, V, E) = -\frac{\mu M}{T} + \frac{pV}{T} + \frac{E}{T}.$$

1 Introducing the specific volume $\tau = V/M$ and the specific internal energy $e = E/M$,
 2 and using the homogeneity of the extensive entropy function, one can define the
 3 specific entropy s

$$(9) \quad s(\tau, e) = S\left(1, \frac{V}{M}, \frac{E}{M}\right) = \frac{1}{M}S(M, V, E).$$

4 The dimensions of the arguments of the extensive entropy S are respectively kg ,
 5 m^3 and J . This is not the case for the middle term in (9) by abuse of notation.

6 We keep the same notations to denote the pressure and the temperature expressed
 7 as functions of the specific volume and energy

$$(10) \quad \frac{1}{T} = \frac{\partial s}{\partial e}(\tau, e), \quad \frac{p}{T} = \frac{\partial s}{\partial \tau}(\tau, e).$$

8 The fundamental thermodynamics relation in its intensive form reads as follow

$$(11) \quad Tds = de + pd\tau.$$

9 and the intensive counterpart of relation (8) is

$$(12) \quad Ts = -\mu + p\tau + e.$$

10 **2.2. The van der Waals Equation of State.** In this work we focus on a non
 11 necessarily concave nor convex entropy function s . A common example is the van
 12 der Waals Equation of State (EoS), with the entropy function

$$(13) \quad s(\tau, e) = C_v \ln\left(\frac{a}{\tau} + e\right) + R \ln(\tau - b) + s_0,$$

13 where R is the universal constant of gas, $C_v > 0$ the calorific constant at constant
 14 volume, s_0 is the entropy of reference, and a and b are two nonnegative parameters
 15 [5, 26].

16 The entropy is well defined for $(\tau, e) \in (\mathbb{R}_*^+)^2$ such that

$$(14) \quad \tau > b, \quad \frac{a}{\tau} + e > 0.$$

17 The corresponding definition domain of s is denoted D_s :

$$(15) \quad D_s := \left\{(\tau, e) \in (\mathbb{R}_*^+)^2; \tau > b \text{ and } \frac{a}{\tau} + e > 0\right\}.$$

18 According to the relations (10), the van der Waals temperature and pressure read

$$(16) \quad T(\tau, e) = \frac{1}{C_v} \left(e + \frac{a}{\tau}\right),$$

$$(17) \quad p(\tau, e) = \frac{R}{C_v(\tau - b)} \left(e + \frac{a}{\tau}\right) - \frac{a}{\tau^2} = \frac{RT(\tau, e)}{\tau - b} - \frac{a}{\tau^2}.$$

19 The van der Waals entropy is neither concave nor convex. Indeed the coefficients
 20 of its Hessian matrix $H_s(\tau, e)$ are given by

$$(18) \quad \begin{cases} \frac{\partial^2 s}{\partial \tau^2}(\tau, e) = \frac{a}{C_v T^2(\tau, e) \tau^3} \left(2C_v T(\tau, e) - \frac{a}{\tau}\right) - \frac{R}{(\tau - b)^2}, \\ \frac{\partial^2 s}{\partial e^2}(\tau, e) = -\frac{1}{C_v T^2(\tau, e)}, \\ \frac{\partial^2 s}{\partial \tau \partial e}(\tau, e) = \frac{1}{C_v T^2(\tau, e)} \frac{a}{\tau^2}. \end{cases}$$

21 Since the temperature T is positive on D_s , one has

$$(19) \quad \frac{\partial^2 s}{\partial e^2} < 0.$$

1 However, the entropy function s is not globally concave and its domain of concavity
 2 restricts to the set where the determinant of H_s is positive, that is

$$(20) \quad D_c := \left\{ (\tau, e) \in D_s; \frac{\partial^2 s}{\partial \tau^2} \frac{\partial^2 s}{\partial e^2} - \left(\frac{\partial^2 s}{\partial e \partial \tau} \right)^2 > 0 \right\}.$$

3 The non-concavity property of the van der Waals entropy makes it an appropriate
 4 toy-model to represent liquid-vapor phase transition [5, chap.9]. States belonging to
 5 the concavity region of the entropy refer to stable and metastable liquid and vapor
 6 states. In contrast states belonging to the non-concavity region are non-admissible
 7 states. The purpose of this section is to precise the geometrical loci of these states
 8 and provide representations of the phase diagrams of the van der Waals EoS in both
 9 the (τ, p) and the (τ, e) planes.

10 Usually the metastable zones of the van der Waals EoS are defined and observable
 11 in the (τ, p) plane at constant temperature. This implies to manipulate the entropy
 12 and the pressure as functions of the volume τ and the temperature T . Adapting
 13 relations (16), (17) and (13) leads to

$$(21) \quad \begin{aligned} s(\tau, T) &= C_v \ln(C_v T) + R \ln(\tau - b) + s_0, \\ p(\tau, T) &= \frac{RT}{\tau - b} - \frac{a}{\tau^2}. \end{aligned}$$

14 We represent in Figure 1 the isothermal curves $(\tau, p(\tau, T))$ (black lines) in the
 15 (τ, p) plane for fixed temperatures T . There exists a unique critical temperature
 16 T_c for which the pressure admits a unique inflection point $(\tau_c, p(\tau_c, T_c))$, called the
 17 critical point. For supercritical temperature $T > T_c$, the pressure is a strictly
 18 decreasing function of the specific volume. Below the critical isothermal curve, for
 19 $T < T_c$, the pressure is an increasing function of the volume between the minimum
 20 $(\tau_-, p(\tau_-, T))$ and the maximum $(\tau_+, p(\tau_+, T))$. This increasing branch refers to
 21 non physically admissible states. The critical isothermal curve is plotted in green in
 22 Figure 1. The set of minima and maxima is plotted in blue in Figure 1 and delimits
 23 the spinodal zone. Actually the spinodal zone in the (τ, p) plane corresponds to the
 24 zone $D_s \setminus D_c$ in the plane (τ, e) where the entropy function is not concave.

25 At a given temperature $T < T_c$, it is classical to replace the non admissible in-
 26 creasing branch of the pressure by a specific isobaric line satisfying the Maxwell
 27 equal area rule. Such a construction defines two volumes τ_1^* and τ_2^* , for each tem-
 28 perature $T < T_c$, such that $p(\tau_1^*, T) = p(\tau_2^*, T)$. Their set, represented in red in
 29 Figure 1, is called the saturation dome. Another classical definition of the saturation
 30 curve is given in Section 3.2, see relations (48). The states belonging to decreasing
 31 branches of isothermal curves, below the saturation dome (in red) and above the
 32 spinodal zone (in blue) are called metastable states.

33 The purpose of this section is to provide a representation of the saturation dome,
 34 spinodal and metastable zones in the (τ, e) plane. We represent in Figure 2 the
 35 isothermal curves in the (τ, e) plane. The spinodal zone corresponds to the domain
 36 where the concavity of the entropy function $(\tau, e) \mapsto s(\tau, e)$ changes. According to
 37 the definition (18) of the Hessian matrix $H_s(\tau, e)$ of the entropy s , this domain is
 38 delimited by the set of states $(\tau, e) \in D_s$ such that

$$(22) \quad \det(H_s)(\tau, e) = 0.$$

39 Solving (22) allows to define the spinodal zone $Z_{\text{Spinodal}} \subset D_s$

$$(23) \quad Z_{\text{Spinodal}} := \{(\tau, e) \in D_s; e < g(\tau)\},$$

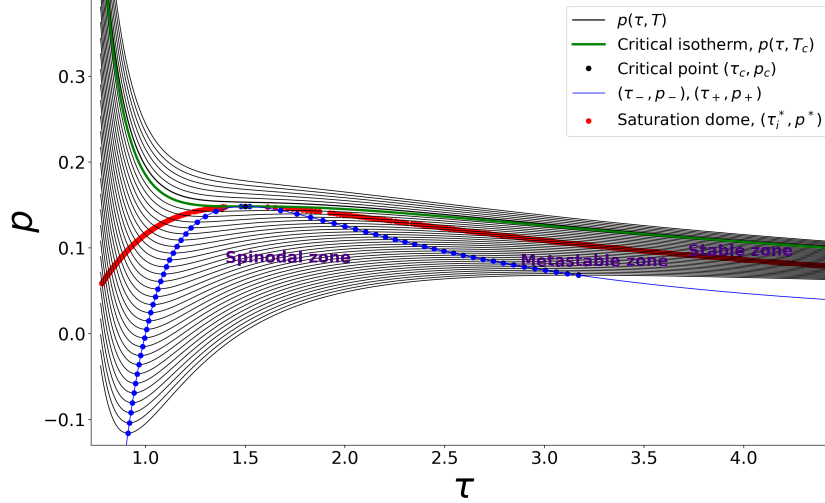


FIGURE 1. Isothermal curves of the van der Waals EoS in the (τ, p) plane. Isothermal curves $p(\tau, T)$ are plotted in black. The isothermal curve at critical temperature $T = T_c$ is plotted in green. Below the critical isothermal curve, the pressure is not monotone with respect to the specific volume and increases in the spinodal zone of non admissible states. This zone is delimited by the blue curve representing the set of minima $(\tau_-, p(\tau_-, T))$ and maxima $(\tau_+, p(\tau_+, T))$ of the pressure for each temperature $T < T_c$. The Maxwell equal area rule construction allows to replace the non physically admissible increasing branch of an isothermal curve by computing two volumes τ_1^* and τ_2^* at each temperature $T < T_c$, such that $p(\tau_1^*, T) = p(\tau_2^*, T)$. The set of these volumes is represented in red in the graph and corresponds to the saturation dome. The states belonging to decreasing branches of isothermal curves, below the saturation dome (in red) and above the spinodal zone (in blue), are called metastable states.

1 where

$$(24) \quad g(\tau) = \frac{2aC_v(\tau - b)^2}{R\tau^3} - \frac{a}{\tau}.$$

2

Remark 1. Classically the spinodal curve is defined as the loci of $\left(\frac{\partial p}{\partial \tau}\right)_T = 0$. Actually it is equivalent to define the spinodal curve as the loci of $\det(H_s)(\tau, e) = 0$. According to (18) the Hessian matrix of $s(\tau, e)$ reads

$$H_s(\tau, e) = \frac{1}{C_v T^2} \begin{pmatrix} \frac{a}{\tau^3}(2C_v T - a/\tau) - \frac{RC_v T^2}{(\tau - b)^2} & \frac{a}{\tau^2} \\ \frac{a}{\tau^2} & -1 \end{pmatrix},$$

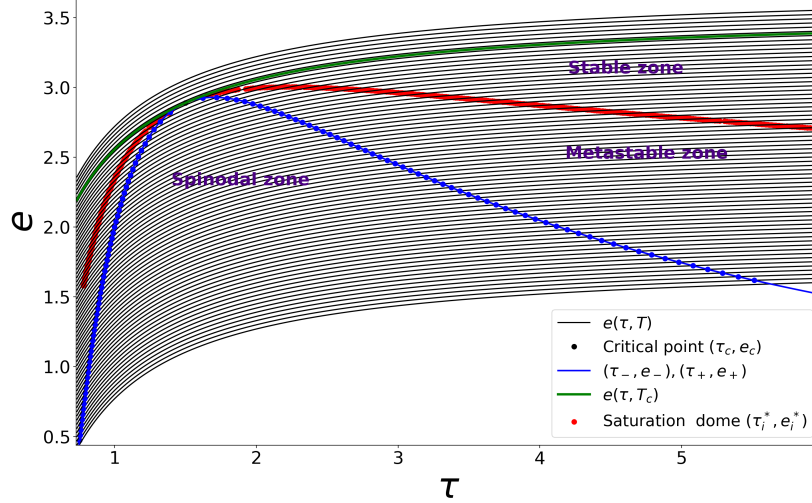


FIGURE 2. Isothermal curves of the van der Waals EoS in the (τ, e) -plane. The black lines correspond to isothermal curves $e(\tau, T)$. The isothermal curve at the critical temperature $T = T_c$ is plotted in green. States belonging to the zone above the critical isothermal curve are supercritical states. The spinodal zone is delimited by the blue curve, which is the graph of the function g defined in (24). The saturation dome is represented by the set of red points. Stable states belong to the areas below the critical isothermal curve (in green) and above the saturation dome (in red). The metastable areas correspond to zones above the spinodal zone (in blue) and below the saturation dome (in red).

where T is a function of (τ, e) . Setting $\det(H_s)(\tau, e) = 0$ gives

$$-C_v T \left(\frac{2a}{\tau^3} - \frac{RT}{(\tau - b)^2} \right) = 0.$$

One observes that the term in parentheses corresponds to the partial derivative of the pressure with respect to the volume at fixed temperature, see (21). Since the temperature is strictly positive, it remains

$$\det(H_s)(\tau, e) = 0 \Leftrightarrow \left(\frac{\partial p}{\partial \tau} \right)_T = 0.$$

1 This equivalent definition allows to determine the minima and maxima of isotherms
 2 and then the spinodal curve in the (τ, p) plane as it is done in [32] and shown in
 3 Figure 1.

4 The critical isothermal curve (green curve) admits a unique intersection point
 5 with the graph of g which turns to be the critical point $(\tau_c, e_c = g(\tau_c))$. In all the
 6 representations given in the sequel, we use a reduced form of the EoS, as the one
 7 proposed in [11], with the parameters

$$(25) \quad a = 1, \quad b = 0.5, \quad R = 0.5, \quad C_v = 3, \quad s_0 = 0,$$

1 which lead to the following critical values

$$(26) \quad \tau_c = 1.5, \quad e_c = 2.88, \quad T_c = 1.185, \quad p_c = 0.148.$$

2 The Maxwell construction, which is usually defined in the (τ, p) -plane, admits
 3 its counterpart in the (τ, e) -plane. Actually the construction of the concave hull of
 4 the van der Waals entropy function $(\tau, e) \mapsto s$ is equivalent to the Maxwell equal
 5 area rule construction [6, 10]. An analogous proof, based on the properties of the
 6 Legendre transform, is available in [19]. In practice, the computation of the concave
 7 hull of the graph of $(\tau, e) \mapsto s$ boils down to the construction of a ruled surface.
 8 For any point (τ, e) , this ruled surface contains a segment which is bitangent to the
 9 graph of $(\tau, e) \mapsto s$ in two points denoted (τ_1^*, e_1^*) and (τ_2^*, e_2^*) . The set of points
 10 $((\tau_1^*, e_1^*), (\tau_2^*, e_2^*))$ defines the saturation dome in the (τ, e) plane and is represented
 11 in red in Figure 2. Note that the computation of the points $((\tau_1^*, e_1^*), (\tau_2^*, e_2^*))$ is not
 12 explicit and requires the resolution of a nonlinear system [6, 10, 19]. However, if we
 13 assume that the set of the red dots is the graph of a function $g^* : \tau \rightarrow g^*(\tau)$, then
 14 the curve $(\tau, g^*(\tau))$ defines the saturation dome $Z_{\text{Saturation}}$, that is

$$(27) \quad Z_{\text{Saturation}} := \{(\tau, e) \in D_s; e = g^*(\tau)\}.$$

15 Thus the metastable states $Z_{\text{Metastable}}$ correspond to the states belonging to the
 16 saturation domain but outside the spinodal zone

$$(28) \quad Z_{\text{Metastable}} := \{(\tau, e) \in D_s; g(\tau) < e < g^*(\tau)\}.$$

17 Finally the stable zones, either stable liquid or stable vapor states, correspond to
 18 states below the critical isotherm curve and above the saturation dome

$$(29) \quad Z_{\text{Stable}} := \{(\tau, e) \in D_s; g^*(\tau) < e < e(\tau, T_c)\}.$$

19 3. THERMODYNAMICS OF EQUILIBRIA FOR A MULTICOMPONENT SYSTEM

20 We consider a system of mass $M > 0$, volume $V > 0$ and energy $E > 0$ which
 21 is composed of I subsystems. Each subsystem $i = 1, \dots, I$ is characterized by its
 22 mass $M_i \geq 0$, its volume $V_i \geq 0$ and its energy $E_i \geq 0$. Moreover, we assume that
 23 each subsystem i follows the same non concave entropy $S(M_i, V_i, E_i)$, namely the
 24 van der Waals EoS in its extensive setting. The conservations of mass and energy
 25 require that

$$(30) \quad M = \sum_{i=1}^I M_i, \quad E = \sum_{i=1}^I E_i.$$

26 Furthermore, we suppose that all the subsystems are immiscible and that no vacuum
 27 appears, in the sense that

$$(31) \quad V = \sum_{i=1}^I V_i.$$

The entropy of the system is the sum of the partial entropies of each subsystem:

$$(M_i, V_i, E_i)_{i=1, \dots, I} \mapsto \sum_{i=1}^I S(M_i, V_i, E_i).$$

28 According to the second principle of thermodynamics, the entropy of the multicomponent
 29 system achieves its maximum at Thermodynamic equilibrium. Considering

1 a state vector (M, V, E) of the multicomponent system, the equilibrium entropy is

$$(32) \quad \Sigma(M, V, E) = \sup_{(M_i, V_i, E_i) \in (\mathbb{R}^+)^3} \sum_{i=1}^I S(M_i, V_i, E_i),$$

2 under the constraints (30)-(31).

3 We now turn to the intensive formulation of the maximization problem. In the
4 following, we denote $\varphi_i = M_i/M \in [0, 1]$ the mass fraction, $\alpha_i = V_i/V \in [0, 1]$ the
5 volume fraction and $\xi_i = E_i/E \in [0, 1]$ the energy fraction. Given $\tau = V/M$ and
6 $e = E/M$ the specific volume and specific energy of the multicomponent system,
7 the specific volume of the subsystem $i = 1, \dots, I$ is $\tau_i = V_i/M_i = \alpha_i \tau / \varphi_i \geq 0$ and
8 its specific energy is $e_i = E_i/M_i = \xi_i e / \varphi_i \geq 0$.

9 The conservation of mass and energy and the volume constraints read now

$$(33) \quad \sum_{i=1}^I \varphi_i = 1, \quad \sum_{i=1}^I \varphi_i \tau_i = \tau, \quad \sum_{i=1}^I \varphi_i e_i = e.$$

10 Using the homogeneity property of the extensive entropy function S , the defini-
11 tions of the mass fractions φ_i and phasic intensive quantities τ_i and e_i , the intensive
12 form of the equilibrium entropy of the system is, for any state vector (τ, e)

$$(34) \quad \sigma(\tau, e) = \sup_{(\tau_i, e_i) \in (\mathbb{R}^+)^2} \sum_{i=1}^I \varphi_i s(\tau_i, e_i),$$

13 under the constraints (33).

14 **3.1. The Gibbs phase rule.** For the moment the number I of subsystems, po-
15 tentially present at the thermodynamic equilibrium, is not determined. Actually,
16 the theorem of Caratheodory gives a first estimate on the number of subsystems I .
17 We recall the theorem statement and refer to [30, 20] for a detailed proof.

18 **Theorem 1.** (Theorem of Caratheodory) Let A be a subset in \mathbb{R}^n and $\text{conv}(A)$ the
19 set of all the convex combinations of elements of A . Then every point $x \in \text{conv}(A)$
20 can be represented as a convex combination of $(n + 1)$ points of A .

21 In the present context, the theorem provides the following first bound.

22 **Proposition 1.** Consider the maximization problem (34) under the constraints
23 (33). The number of subsystems which may coexist at equilibrium is $I \leq 3$.

24 *Proof.* Consider $(\tau, e) \in (\mathbb{R}^+)^2 \mapsto -s(\tau, e) \in \mathbb{R}$. According to Caratheodory's
25 theorem, the convex hull of the epigraph of $-s$ at any point $(\tau, e) \in (\mathbb{R}^+)^2$ is

$$(35) \quad (\text{conv}(-s))(\tau, e) = \inf \sum_{i=1}^3 -\lambda_i s(\tau_i, e_i),$$

26 with $\sum_{i=1}^3 \lambda_i \tau_i = \tau$ and $\sum_{i=1}^3 \lambda_i e_i = e$ where the infimum is taken over all the expressions
27 of (τ, e) as a convex combinations of three points (τ_i, e_i) , $i = 1, 2, 3$. Now considering
28 $\lambda_i = \varphi_i$, we recover the intensive constraints (33) and the maximization problem
29 (34) is equivalent to the determination of the concave hull of s . \square

30 As a consequence of Caratheodory's Theorem, at the most three phases remain
31 at thermodynamic equilibrium. This result is in total agreement with the Gibbs
32 phase rule. Indeed, considering a single component system, the Gibbs phase rule

1 states that the number of phases is $I = 3 - F$, where $F \geq 0$ is the degree of freedom
2 [2, 28].

3 Actually when considering the van der Waals EoS, the admissible number of
4 subsystems present at Thermodynamic equilibrium restricts to at most 2.

5 **Theorem 2.** Consider the maximization problem (34), and assume that the entropy
6 function s verifies the inequality (19). Then

$$(36) \quad I(\tau, e) < 3 \quad \forall (\tau, e) \in D_s.$$

7 *Proof.* Assume that $I = 3$ and consider a point $X \in D_s$. Then X belongs to a
8 simplex of dimension 2. On the one hand, inside this simplex, the concave hull
9 of s , denoted $\text{conc}(s)$ is an affine function. It follows that the partial derivatives
10 of $\text{conc}(s)$, $\partial_\tau \text{conc}(s)(X)$ and $\partial_e \text{conc}(s)(X)$ are constant. On the other hand, at
11 the boundaries of the simplex, the concave hull $\text{conc}(s)$ is tangent to the surface
12 $(\tau, e) \mapsto s$. Hence $\partial_e \text{conc}(s)(X) = \partial_e s(X)$, which leads to a contradiction with
13 property (19). \square

14 According to Theorem 2, the maximization process using the van der Waals EoS
15 does not allow the coexistence of more than two phases and prevents from the
16 modelling of a triple point.

17 **3.2. Maxima of the constrained optimization problem.** From now on we
18 consider $I = 2$ and consider the optimization problem

$$(37) \quad \sigma(\tau, e) = \max \mathcal{S}(\varphi_1, \varphi_2, \tau_1, \tau_2, e_1, e_2),$$

19 where

$$(38) \quad \mathcal{S}(\varphi_1, \varphi_2, \tau_1, \tau_2, e_1, e_2) = \varphi_1 s(\tau_1, e_1) + \varphi_2 s(\tau_2, e_2),$$

20 under the constraints

$$(39) \quad \varphi_1 + \varphi_2 = 1, \quad \varphi_1 \tau_1 + \varphi_2 \tau_2 = \tau, \quad \varphi_1 e_1 + \varphi_2 e_2 = e.$$

21 Note that if $\tau_1 \neq \tau_2$ and $e_1 \neq e_2$, (39) imply that the mass fractions φ_i , $i = 1, 2$
22 satisfy

$$(40) \quad \varphi_1 = \frac{\tau - \tau_2}{\tau_1 - \tau_2} = \frac{e - e_2}{e_1 - e_2}, \quad \varphi_2 = \frac{\tau - \tau_1}{\tau_2 - \tau_1} = \frac{e - e_1}{e_2 - e_1}.$$

23 On the other hand, if $\tau = \tau_1 = \tau_2$ and $e = e_1 = e_2$, the mass fraction is undeter-
24 mined. In order to preserve the positivity of the fractions, we assume that

$$(41) \quad (\tau, e) \in [\min(\tau_1, \tau_2), \max(\tau_1, \tau_2)] \times [\min(e_1, e_2), \max(e_1, e_2)].$$

25 Introducing the Lagrange multipliers λ_φ , λ_τ and λ_e associated to the constraints
26 (39), we define the Lagrangian

$$(42) \quad L(\lambda_\varphi, \lambda_\tau, \lambda_e, x) = \mathcal{S}(x) + \lambda_\varphi \beta_\varphi(x) + \lambda_\tau \beta_\tau(x) + \lambda_e \beta_e(x),$$

27 with $x = (\varphi_1, \varphi_2, \tau_1, \tau_2, e_1, e_2)$ and

$$(43) \quad \begin{cases} \beta_\varphi(x) = \varphi_1 + \varphi_2 - 1, \\ \beta_\tau(x) = \varphi_1 \tau_1 + \varphi_2 \tau_2 - \tau, \\ \beta_e(x) = \varphi_1 e_1 + \varphi_2 e_2 - e. \end{cases}$$

Since \mathcal{S} is C^1 and the conditions (43) are affine, we obtain straightforwardly the optimality conditions for the maxima in the problem (37)-(39):

$$(44a) \quad s(\tau_1, e_1) + \lambda_\varphi + \lambda_\tau \tau_1 + \lambda_e e_1 = 0,$$

$$(44b) \quad s(\tau_2, e_2) + \lambda_\varphi + \lambda_\tau \tau_2 + \lambda_e e_2 = 0,$$

$$(44c) \quad \varphi_1 \frac{p(\tau_1, e_1)}{T(\tau_1, e_1)} + \varphi_1 \lambda_\tau = 0,$$

$$(44d) \quad \varphi_2 \frac{p(\tau_2, e_2)}{T(\tau_2, e_2)} + \varphi_2 \lambda_\tau = 0,$$

$$(44e) \quad \varphi_1 \frac{1}{T(\tau_1, e_1)} + \varphi_1 \lambda_e = 0,$$

$$(44f) \quad \varphi_2 \frac{1}{T(\tau_2, e_2)} + \varphi_2 \lambda_e = 0.$$

1 We now turn to the determination of the maxima of the problem (37). It turns out
 2 that it involves the notion of relative entropy, which is defined, for any two states
 3 $a, b \in (\mathbb{R}^+)^2$ by

$$(45) \quad s(a|b) = s(a) - s(b) - \nabla s(b) \cdot (a - b).$$

4 **Proposition 2.** The maxima of the problem (37)-(39) are

5 (1) **Identification of phases 1 and 2:**

- 6 • $\tau_1 = \tau_2 = \tau$ and $e_1 = e_2 = e$, φ_i undetermined,
 7 • $\varphi_1 = 0$, $\varphi_2 = 1$, $(\tau_2, e_2) = (\tau, e)$ and (τ_1, e_1) solution to

$$(46) \quad \begin{cases} s((\tau_1, e_1)|(\tau, e)) & = 0, \\ \mu(\tau_1, e_1)/T(\tau_1, e_1) & = \mu(\tau, e)/T(\tau, e). \end{cases}$$

- 8 • $\varphi_1 = 1$, $\varphi_2 = 0$, $(\tau_1, e_1) = (\tau, e)$ and (τ_2, e_2) solution to

$$(47) \quad \begin{cases} s((\tau_2, e_2)|(\tau, e)) & = 0, \\ \mu(\tau_2, e_2)/T(\tau_2, e_2) & = \mu(\tau, e)/T(\tau, e). \end{cases}$$

9 (2) **Saturation states:** there exists a unique couple of points

10 $M_1^* = (\tau_1^*, e_1^*, s(\tau_1^*, e_1^*))$ and $M_2^* = (\tau_2^*, e_2^*, s(\tau_2^*, e_2^*))$
 11 with $\tau \in [\min(\tau_1^*, \tau_2^*), \max(\tau_1^*, \tau_2^*)]$ and $e \in [\min(e_1^*, e_2^*), \max(e_1^*, e_2^*)]$ given
 12 by (40), satisfying

$$(48) \quad \begin{cases} p(\tau_1^*, e_1^*) = p(\tau_2^*, e_2^*), \\ \mu(\tau_1^*, e_1^*) = \mu(\tau_2^*, e_2^*), \\ T(\tau_1^*, e_1^*) = T(\tau_2^*, e_2^*), \end{cases}$$

13 such that $M = (\tau, e, \sigma(\tau, e))$ belongs to the line open segment $(M_1^*, M_2^*) =$
 14 $\{zM_1^* + (1-z)M_2^*, z \in]0, 1[\}$ contained in the concave hull $\text{conc}(s)$.

15 In Proposition 2- 2, taking $z = 0$ or $z = 1$ corresponds to Proposition 2- 1. Since
 16 item 2 characterizes the saturation states, that is liquid-vapor mixture, one does not
 17 consider the configuration where $(\tau_1^*, e_1^*) = (\tau_2^*, e_2^*) = (\tau, e)$ obtained when $z = 0$ or
 18 $z = 1$.

Proof. The first case $\tau = \tau_1 = \tau_2$ and $e = e_1 = e_2$ is straightforward. We focus on
 the case $\varphi_1 = 0$. The mass conservation constraint induces $\varphi_2 = 1$ and thus $\tau_2 = \tau$

and $e_2 = e$. Then the optimality conditions (44d) and (44f) give

$$\lambda_\tau = -p(\tau, e)/T(\tau, e), \quad \lambda_e = -1/T(\tau, e).$$

1 Associated with the conditions (44a) and (44b), the definition of the relative
2 entropy (45) and the definition of the chemical potential (12), one determines (τ_1, e_1)
3 as the solution of (46). The same holds for the case $\varphi_1 = 1$.

We now consider the saturation case. It is characterized by $\varphi_1\varphi_2 \neq 0$. The optimization procedure also reads as a convexification of $(\tau, e) \mapsto s(\tau, e)$ in the sense that the graph of $(\tau, e) \mapsto \sigma(\tau, e)$ is the concave hull of $(\tau, e) \mapsto s(\tau, e)$, see the definition (35). Then for any saturation state (τ, e) , the graph of σ contains a segment $(M_1^*M_2^*)$ passing through $(\tau, e, \sigma(\tau, e))$. The characterization (48) of the points M_1^* and M_2^* derives from the optimality conditions. Combining (44e) and (44f) gives the temperatures equality

$$\frac{1}{T(\tau_1^*, e_1^*)} = \frac{1}{T(\tau_2^*, e_2^*)}.$$

Similarly using (44c) and (44d), yields

$$\frac{p(\tau_1^*, e_1^*)}{T(\tau_1^*, e_1^*)} = \frac{p(\tau_2^*, e_2^*)}{T(\tau_2^*, e_2^*)}.$$

Finally (44a) and (44b), combined with the definition of the chemical potential (12), give

$$\frac{\mu(\tau_1^*, e_1^*)}{T(\tau_1^*, e_1^*)} = \frac{\mu(\tau_2^*, e_2^*)}{T(\tau_2^*, e_2^*)}.$$

4 We now address the uniqueness of the segment $(M_1^*M_2^*)$. Outside the spinodal
5 zone, the van der Waals entropy is a concave and increasing function with respect
6 to τ and e . Then there is a bijection between (p, T) and (τ_i, e_i) , $i = 1, 2$. Define a
7 second segment $(\widetilde{M}_1^*\widetilde{M}_2^*)$ with $\widetilde{M}_1^* = (\widetilde{\tau}_1^*, \widetilde{e}_1^*)$ and $\widetilde{M}_2^* = (\widetilde{\tau}_2^*, \widetilde{e}_2^*)$. If $(\tau, e, \sigma(\tau, e)) \in$
8 $(M_1^*M_2^*) \cap (\widetilde{M}_1^*\widetilde{M}_2^*)$, since (p, T, μ) are constant along $(M_1^*M_2^*)$ and $(\widetilde{M}_1^*\widetilde{M}_2^*)$, then
9 $M_i^* = \widetilde{M}_i^*$ and the segments coincide. \square

10 Notice that, for a given saturation state (τ, e) , the quadruplet $(\tau_1^*, \tau_2^*, e_1^*, e_2^*)$
11 satisfies also

$$(49) \quad s((\tau_1^*, e_1^*)|(\tau_2^*, e_2^*)) = s((\tau_2^*, e_2^*)|(\tau_1^*, e_1^*)) = 0.$$

12 We emphasize that the necessary conditions in Proposition 2 include all equilib-
13 rium states, regardless of their stability. In particular, we recover in item (1) the
14 complete van der Waals EoS, including physically unstable states (spinodal zone),
15 and liquid and vapor metastable and stable states.

16 To proceed further the classical method consists in studying the local concavity
17 of the mixture entropy out equilibrium \mathcal{S} introduced in (38). We adopt here the
18 approach proposed in [24]. We introduce a relaxation towards the equilibrium states
19 by means of a dynamical system.

20 4. DYNAMICAL SYSTEM AND ATTRACTION BASSINS

21 The goal of this section is to introduce time dependence to create a dynamical
22 system able to characterize all the equilibrium states including the metastable states.
23 To build the appropriate dynamical system, we impose two basic criteria:

- 24 • long-time equilibria coincide with the maxima given by the optimality con-
25 ditions in Proposition 2.

1 • the mixture entropy increases along trajectories.

2 Fix (τ, e) a state vector of the system. The maximization problem applies to
 3 six variables under the three constraints (39). Hence it is sufficient to reduce the
 4 variables from six to three. We consider the vector of volume, mass and energy
 5 fractions $\mathbf{r} = (\alpha, \varphi, \xi)$. Then the phasic specific energies and volumes are now
 6 functions of $\mathbf{r} = (\alpha, \varphi, \xi) \in]0, 1[^3$ with

$$(50) \quad \begin{aligned} \tau_1(\mathbf{r}) &= \frac{\alpha\tau}{\varphi}, & \tau_2(\mathbf{r}) &= \frac{(1-\alpha)\tau}{1-\varphi}, \\ e_1(\mathbf{r}) &= \frac{\xi e}{\varphi}, & e_2(\mathbf{r}) &= \frac{(1-\xi)e}{1-\varphi}. \end{aligned}$$

7 The formulas in (50) do not suggest any natural order in the volumes nor energies.
 8 Besides, it is possible that the phasic specific volumes (resp. energies) coincide.
 9 Indeed, if $\alpha = \varphi = \xi \in]0, 1[$, then $\tau_1(\mathbf{r}) = \tau_2(\mathbf{r}) = \tau$ and $e_1(\mathbf{r}) = e_2(\mathbf{r}) = e$. Hence
 10 the constraint (41) still remains.

11 In this context, the mixture entropy of the system becomes a function of \mathbf{r} , still
 12 denoted \mathcal{S} :

$$(51) \quad \mathcal{S}(\mathbf{r}) = \varphi s(\tau_1(\mathbf{r}), e_1(\mathbf{r})) + (1-\varphi)s(\tau_2(\mathbf{r}), e_2(\mathbf{r})).$$

13 Using the relations (50) and the expressions (10) of the partial derivatives of the
 14 entropy function, the gradient of \mathcal{S} reads

$$(52) \quad \nabla_{\mathbf{r}}\mathcal{S}(\mathbf{r}) = \begin{pmatrix} \tau \frac{p(\tau_1(\mathbf{r}), e_1(\mathbf{r}))}{T(\tau_1(\mathbf{r}), e_1(\mathbf{r}))} - \tau \frac{p(\tau_2(\mathbf{r}), e_2(\mathbf{r}))}{T(\tau_2(\mathbf{r}), e_2(\mathbf{r}))} \\ -\frac{\mu(\tau_1(\mathbf{r}), e_1(\mathbf{r}))}{T(\tau_1(\mathbf{r}), e_1(\mathbf{r}))} + \frac{\mu(\tau_2(\mathbf{r}), e_2(\mathbf{r}))}{T(\tau_2(\mathbf{r}), e_2(\mathbf{r}))} \\ \frac{1}{T(\tau_1(\mathbf{r}), e_1(\mathbf{r}))} - \frac{1}{T(\tau_2(\mathbf{r}), e_2(\mathbf{r}))} \end{pmatrix}.$$

15 Observe that both \mathcal{S} and $\nabla_{\mathbf{r}}\mathcal{S}$ are defined only for $(\alpha, \varphi, \xi) \in]0, 1[^3$.

16 We wish to construct a dynamical system which complies with the entropy
 17 growth criterion in the sense that entropy increases along the trajectories *i.e.*
 18 $d/dt\mathcal{S}(\mathbf{r}(t)) \geq 0$. A naive choice is to choose $\dot{\mathbf{r}}$ close to $\nabla_{\mathbf{r}}\mathcal{S}$. We introduce
 19 the following dynamical system:

$$(53) \quad \begin{cases} \dot{\alpha}(t) = \alpha(1-\alpha)\tau \left(\frac{p(\tau_1(\mathbf{r}), e_1(\mathbf{r}))}{T(\tau_1(\mathbf{r}), e_1(\mathbf{r}))} - \frac{p(\tau_2(\mathbf{r}), e_2(\mathbf{r}))}{T(\tau_2(\mathbf{r}), e_2(\mathbf{r}))} \right), \\ \dot{\varphi}(t) = \varphi(1-\varphi) \left(\frac{\mu(\tau_2(\mathbf{r}), e_2(\mathbf{r}))}{T(\tau_2(\mathbf{r}), e_2(\mathbf{r}))} - \frac{\mu(\tau_1(\mathbf{r}), e_1(\mathbf{r}))}{T(\tau_1(\mathbf{r}), e_1(\mathbf{r}))} \right), \\ \dot{\xi}(t) = \xi(1-\xi)e \left(\frac{1}{T(\tau_1(\mathbf{r}), e_1(\mathbf{r}))} - \frac{1}{T(\tau_2(\mathbf{r}), e_2(\mathbf{r}))} \right). \end{cases}$$

20 **Proposition 3.** The dynamical system (53) satisfies the following properties.

- 21 (1) If $\mathbf{r}(0) \in]0, 1[^3$ then, for all time $t > 0$, one has $\mathbf{r}(t) \in]0, 1[^3$.
 22 (2) If the condition (41) is satisfied at $t = 0$, then (τ, e) belongs to the segment
 23 $[(\tau_1(\mathbf{r}), e_1(\mathbf{r}))(t), (\tau_2(\mathbf{r}), e_2(\mathbf{r}))(t)]$ for all time $t > 0$.
 24 (3) The mixture entropy increases along the trajectories

$$(54) \quad \frac{d}{dt}\mathcal{S}(\mathbf{r}(t)) \geq 0.$$

Proof. The multiplicative term $\alpha(1-\alpha)$ in the first equation of (53) ensures that the
 right-hand side vanishes only if the term $\left| \frac{p(\tau_1(\mathbf{r}), e_1(\mathbf{r}))}{T(\tau_1(\mathbf{r}), e_1(\mathbf{r}))} - \frac{p(\tau_2(\mathbf{r}), e_2(\mathbf{r}))}{T(\tau_2(\mathbf{r}), e_2(\mathbf{r}))} \right|$ remains

bounded when α tends to 0 or 1. The same holds for the equations on the remaining fractions φ and ξ . This proves (1). Item (2) is nothing but a reformulation of (40). Finally, the time derivative of the mixture entropy writes

$$\frac{d}{dt}\mathcal{S}(\mathbf{r}(t)) = \nabla\mathcal{S}(\mathbf{r}) \cdot \dot{\mathbf{r}}(t).$$

1 Since $\tau > 0$, $e > 0$ and the fractions belong to $]0, 1[$, it follows that the item (3)
2 holds true. \square

3 **4.1. Equilibria and attractivity.** In the sequel, we let $\mathbb{F}(\mathbf{r}) = (\mathbb{F}^\alpha, \mathbb{F}^\varphi, \mathbb{F}^\xi)$ be the
4 right-hand side of (53), such that

$$(55) \quad \begin{cases} \dot{\alpha}(t) = \mathbb{F}^\alpha(\mathbf{r}), \\ \dot{\varphi}(t) = \mathbb{F}^\varphi(\mathbf{r}), \\ \dot{\xi}(t) = \mathbb{F}^\xi(\mathbf{r}). \end{cases}$$

5 **Proposition 4** (Equilibrium states). The equilibrium states for the dynamical
6 system (53) are

- 7 (1) Saturation states: either $\mathbf{r}^* = (\alpha^*, \varphi^*, \xi^*)$ or $\mathbf{r}^\# = (1 - \alpha^*, 1 - \varphi^*, 1 - \xi^*)$ with
8 $\alpha^* \neq \varphi^* \neq \xi^* \in]0, 1[$, defined by (50) such that $\tau_i^* = \tau_i(\mathbf{r}^*) = \tau_i(\mathbf{r}^\#)$ and
9 $e_i^* = e_i(\mathbf{r}^*) = e_i(\mathbf{r}^\#)$, $i = 1, 2$, corresponding to the characterization (48) of
10 Proposition 2- (2).
11 (2) Identification of phases 1 and 2: $\bar{\mathbf{r}} = (\beta, \beta, \beta)$, $\beta \in]0, 1[$ such that $\tau_1(\bar{\mathbf{r}}) =$
12 $\tau_2(\bar{\mathbf{r}}) = \tau$ and $e_1(\bar{\mathbf{r}}) = e_2(\bar{\mathbf{r}}) = e$.

13 The equilibria of the dynamical system are given by $\mathbb{F}(\mathbf{r}) = 0$. In the case of
14 equilibria (1), consider that $\alpha \neq \varphi \neq \xi$. Then, according to the Proposition 2- (2),
15 there exists a unique triplet $r^* = (\alpha^*, \varphi^*, \xi^*)$ such that the characterization (48)
16 holds. It turns out that $\mathbf{r}^\#$ is also an equilibrium of the system. If the equilibrium
17 r^* corresponds to $\tau_1^* < \tau < \tau_2^*$, $e_1^* < e < e_2^*$, then the equilibrium $\mathbf{r}^\#$ corresponds
18 to $\tau_1^* > \tau > \tau_2^*$ and $e_1^* > e > e_2^*$ and conversely.

19 Both \mathbf{r}^* and $\mathbf{r}^\#$ are equilibrium states since the two phases have the same EOS
20 and, thus, they can be swapped.

21 In the case of equilibria (2), the two phases coincide, in the sense that $\tau_1 = \tau_2 = \tau$
22 and $e_1 = e_2 = e$. The determination of the constant $\beta \in]0, 1[$ depends on the initial
23 data of the dynamical system (53). We emphasize that the equilibrium states
24 $\mathbf{r} = (\beta, \beta, \beta)$ are valid for all states (τ, e) and go over the van der Waals surface. In
25 other words, all states $(\tau, e, s(\tau, e))$ of the van der Waals surface are solutions of the
26 optimization problem (37). Especially the pure liquid-vapor states, the metastable
27 states but also unstable states of the spinodal zone are equilibria.

28 Therefore, to go further and identify the physically admissible equilibrium states,
29 we must investigate their stability and attractivity.

30 **Proposition 5** (Attractivity). The equilibrium states are classified as follow:

- 31 • The saturation states $\mathbf{r}^* = (\alpha^*, \varphi^*, \xi^*)$ and $\mathbf{r}^\# = (1 - \alpha^*, 1 - \varphi^*, 1 - \xi^*)$ are
32 attractive points,
33 • The equilibrium $\bar{\mathbf{r}} = (\beta, \beta, \beta) \in]0, 1[$, corresponding to the identification of
34 the two phases, is strongly degenerate.

Proof. We deal with the proof of the second item. The attractivity of the equilib-
rium states \mathbf{r}^* and $\mathbf{r}^\#$ is difficult to prove because the eigenvalues of the Jacobian

matrix of \mathbb{F} do not simplify. We give in Remark 2 numerical evidence for the attractiveness of the equilibrium states \mathbf{r}^* and $\mathbf{r}^\#$. In the sequel and for sake of readability, we denote $p_i := p(\tau_i(\mathbf{r}), e_i(\mathbf{r}))$, $T_i := T(\tau_i(\mathbf{r}), e_i(\mathbf{r}))$ and $\mu_i := \mu(\tau_i(\mathbf{r}), e_i(\mathbf{r}))$. The goal now is to find the spectrum of the Jacobian matrix of \mathbb{F} denoted by

$$D_{\mathbf{r}}\mathbb{F}(\mathbf{r}) := \begin{pmatrix} \partial_\alpha \mathbb{F}^\alpha(\mathbf{r}) & \partial_\varphi \mathbb{F}^\alpha(\mathbf{r}) & \partial_\xi \mathbb{F}^\alpha(\mathbf{r}) \\ \partial_\alpha \mathbb{F}^\varphi(\mathbf{r}) & \partial_\varphi \mathbb{F}^\varphi(\mathbf{r}) & \partial_\xi \mathbb{F}^\varphi(\mathbf{r}) \\ \partial_\alpha \mathbb{F}^\xi(\mathbf{r}) & \partial_\varphi \mathbb{F}^\xi(\mathbf{r}) & \partial_\xi \mathbb{F}^\xi(\mathbf{r}) \end{pmatrix}.$$

- 1 Consider the equilibrium $\bar{\mathbf{r}} = (\beta, \beta, \beta) \in]0, 1[^3$, which corresponds to the identifica-
 2 tion of the two phases. In that case, the Jacobian matrix $D_{\bar{\mathbf{r}}}\mathbb{F}(\bar{\mathbf{r}})$ reads
 (56)

$$D_{\bar{\mathbf{r}}}\mathbb{F}(\bar{\mathbf{r}}) = \begin{pmatrix} \tau \partial_\tau \left(\frac{p}{T}\right)(\tau, e) & -\tau \partial_\tau \left(\frac{p}{T}\right)(\tau, e) - e \partial_e \left(\frac{p}{T}\right)(\tau, e) & e \partial_e \left(\frac{p}{T}\right)(\tau, e) \\ -\tau \partial_\tau \left(\frac{\mu}{T}\right)(\tau, e) & \tau \partial_\tau \left(\frac{\mu}{T}\right)(\tau, e) + e \partial_e \left(\frac{\mu}{T}\right)(\tau, e) & -e \partial_e \left(\frac{\mu}{T}\right)(\tau, e) \\ \tau \partial_\tau \left(\frac{1}{T}\right)(\tau, e) & -\tau \partial_\tau \left(\frac{1}{T}\right)(\tau, e) - e \partial_e \left(\frac{1}{T}\right)(\tau, e) & e \partial_e \left(\frac{1}{T}\right)(\tau, e) \end{pmatrix}.$$

- 3 Since the middle column is the opposite of the sum of the two remaining columns,
 4 then the determinant of $D_{\bar{\mathbf{r}}}\mathbb{F}(\bar{\mathbf{r}})$ is zero and the Jacobian matrix admits a null
 5 eigenvalue. Hence the equilibrium $\bar{\mathbf{r}}$ is a strongly degenerate. \square

- 6 **Remark 2.** As the saturation equilibrium $\mathbf{r}^* = (\alpha^*, \varphi^*, \xi^*)$ is concerned, the co-
 7 efficients of the Jacobian matrix $D_{\mathbf{r}}\mathbb{F}(\mathbf{r}^*)$ do not simplify much and obtaining an
 8 explicit formulation of its eigenvalues is out of reach. So, we turn to the numerical
 9 illustration of the spectrum $\{\lambda_1, \lambda_2, \lambda_3\}$ of the matrix $D_{\mathbf{r}}\mathbb{F}(\mathbf{r}^*)$ for some saturation
 10 states $\mathbf{r}^* = (\alpha^*, \varphi^*, \xi^*)$ with the van der Waals EoS with parameters (25).

\mathbf{r}^*	(τ, e)	(τ_1^*, e_1^*)	(τ_2^*, e_2^*)	λ_1	λ_2	λ_3
(0.71, 0.29, 0.39)	(1.99, 2.1)	(4.76, 2.80)	(0.82, 1.80)	-8.443	-1.290	-0.061
(0.94, 0.73, 0.82)	(3.9, 2.49)	(5.13, 2.77)	(0.81, 1.73)	-5.713	2.048	-0.055
(0.76, 0.22, 0.35)	(2.39, 1.59)	(8.23, 2.56)	(0.73, 1.32)	-8.477	-2.835	-0.110
(0.64, 0.14, 0.24)	(1.79, 1.49)	(8.25, 2.56)	(0.73, 1.32)	-9.044	-2.405	-0.097
(0.68, 0.25, 0.35)	(1.89, 1.99)	(5.11, 2.77)	(0.81, 1.73)	-8.660	-1.368	-0.065

- 11 One observes numerically that, for these saturation equilibria \mathbf{r}^* , the Jacobian ma-
 12 trix $D_{\mathbf{r}}\mathbb{F}(\mathbf{r}^*)$ admits three negative eigenvalues, which means that these equilibria
 13 are attractive. The same hold true for the equilibrium $\mathbf{r}^\#$.

- 14 To complete the study of equilibrium states, in particular to cope with the degen-
 15 erate state $\bar{\mathbf{r}}$, corresponding to the identification of the two phases, we investigate
 16 the attraction basins of $\bar{\mathbf{r}}$, \mathbf{r}^* and $\mathbf{r}^\#$. We introduce the following functions with
 17 index I for Identification and S for Saturation:

$$(57) \quad \begin{aligned} G_S(\mathbf{r}) &= -\mathcal{S}(\mathbf{r}) + \text{conc}(s)(\tau, e), \\ G_I(\mathbf{r}) &= -\mathcal{S}(\mathbf{r}) + s(\tau, e), \end{aligned}$$

- 18 where $\text{conc}(s)(\tau, e)$ refers to the concave hull of the function s , see the definition
 19 (35).

- 20 **Proposition 6.** The basins of attraction of the equilibrium states are the following:

- 21 • In the spinodal zone, with $(\tau, e) \in Z_{\text{Spinodal}}$, G_S is a Lyapunov function on
 22 the whole domain $(\alpha, \varphi, \xi) \in]0, 1[^3$.

1 • In the liquid or vapor stable zones, with $(\tau, e) \in Z_{\text{Stable}}$, G_I is a Lyapunov
2 function of the whole domain $(\alpha, \varphi, \xi) \in]0, 1[^3$.

3 *Proof.* The two functions are candidate to be a Lyapunov function, since

• by construction $G_S(\mathbf{r}^*) = 0$. Indeed, the concerning equilibrium state is

$$\mathbf{r}^* = (\alpha^*, \varphi^*, \xi^*) = \left(\frac{\varphi^* \tau_1^*}{\tau}, \varphi^*, \frac{\varphi^* e_1^*}{e} \right)$$

where (τ_1^*, e_1^*) , (τ_2^*, e_2^*) are characterized by proposition 2-2 and φ^* satisfies
(40) and takes the following expression

$$\varphi^* = \frac{\tau - \tau_2^*}{\tau_1^* - \tau_2^*} = \frac{e - e_2^*}{e_1^* - e_2^*}.$$

4 Denoting $p^* = p(\tau_1^*, e_1^*) = p(\tau_1^*, e_2^*)$, $T^* = T(\tau_1^*, e_1^*) = T(\tau_1^*, e_2^*)$, and
5 $\mu^* = \mu(\tau_1^*, e_1^*) = \mu(\tau_1^*, e_2^*)$, one has

$$\begin{aligned} (58) \quad G_S(\mathbf{r}^*) &= -\varphi^* s(\tau_1^*, e_1^*) - (1 - \varphi^*) s(\tau_2^*, e_2^*) + p^*/T^* \tau + e/T^* + \mu^*/T^* \\ &= p^*/T^* (\tau - \varphi^* \tau_1^* - (1 - \varphi^*) \tau_2^*) + 1/T^* (e - \varphi^* e_1^* - (1 - \varphi^*) e_2^*) \\ &\quad + \mu^*/T^* (1 - \varphi^* - (1 - \varphi^*)) \\ &= 0, \end{aligned}$$

6 using the Gibbs relation (12). The same holds for the equilibrium $\mathbf{r}^\#$.
7 Similarly $G_I(\bar{\mathbf{r}}) = 0$;

8 • it holds $\nabla_{\mathbf{r}} G_S(\mathbf{r}) = \nabla_{\mathbf{r}} G_I(\mathbf{r}) = -\nabla_{\mathbf{r}} \mathcal{S}(\mathbf{r})$. Then we obtain as well $\nabla_{\mathbf{r}} G_S(\mathbf{r}^*) =$
9 $\nabla_{\mathbf{r}} G_S(\mathbf{r}^\#) = \nabla_{\mathbf{r}} G_S(\bar{\mathbf{r}}) = 0$, according to (52);
• for the same reason, and using (54), we have

$$\frac{d}{dt} G_S(\mathbf{r}(t)) = \frac{d}{dt} G_I(\mathbf{r}(t)) \leq 0.$$

10 It remains to check the positivity of G_S and G_I in a neighborhood of \mathbf{r}^* , $\mathbf{r}^\#$ and $\bar{\mathbf{r}}$
11 respectively, depending on the domain the state (τ, e) belongs to.

12 **Saturation** with $(\tau, e) \in Z_{\text{Spinodal}}$. By definition of $\text{conc}(s)$, $\text{conc}(s)(\tau, e) > \mathcal{S}(\mathbf{r})$
13 for $\mathbf{r} \neq \mathbf{r}^*$ (or equivalently $\mathbf{r} \neq \mathbf{r}^\#$). Hence $G_S(\mathbf{r}) > 0$.

Stable states with $(\tau, e) \in Z_{\text{Stable}}$. We make use again of the concave hull of s

$$\begin{aligned} G_I(\mathbf{r}) &= -\varphi s(\alpha/\varphi\tau, \xi/\varphi e) - (1 - \varphi) s((1 - \alpha)/(1 - \varphi)\tau, (1 - \xi)/(1 - \varphi)e) - s(\tau, e) \\ &\geq -\varphi \text{conc}(s)(\alpha/\varphi\tau, \xi/\varphi e) \\ &\quad - (1 - \varphi) \text{conc}(s)((1 - \alpha)/(1 - \varphi)\tau, (1 - \xi)/(1 - \varphi)e) \\ &\quad - s(\tau, e) \\ &\geq -\text{conc}(s)(\alpha/\varphi\tau + (1 - \alpha)/(1 - \varphi)\tau, \xi/\varphi e + (1 - \xi)/(1 - \varphi)e) - s(\tau, e) \\ &= -\text{conc}(s)(\tau, e) - s(\tau, e). \end{aligned}$$

14 In the liquid or vapor stable zones, (τ, e) belongs to the convex hull of the graph
15 of s , that is $\text{conc}(s)(\tau, e) = s(\tau, e)$. Then $G_I(\mathbf{r}) \geq 0$ and the equality occurs if
16 $\mathbf{r} = \bar{\mathbf{r}}$. \square

17 When considering the metastable regions with $(\tau, e) \in Z_{\text{Metastable}}$, there are two
18 basins of attraction, numerically illustrated in Section 4.2.3, see Figure 9. Unlike
19 in the spinodal zone, the function G_I is non-negative in a neighborhood of (τ, e) ,
20 provided that (τ, e) belongs to a zone of strict concavity of s . It means that both
21 $\bar{\mathbf{r}}$ and \mathbf{r}^* are reachable. The two basins of attraction are separated by an unstable

1 manifold, which is difficult to determine theoretically and numerically as well. It
 2 is already tough in the isothermal framework, see [24], [14] and [15]. In the latter
 3 reference the determination of the basins of the metastable states is more precise,
 4 even if it is not explicit, the basins being defined through the application of the
 5 implicit function theorem.

6 **4.2. Numerical illustrations.** This section provides numerical simulations to il-
 7 lustrate the behavior of the dynamical system (53) and the attraction of each pos-
 8 sible equilibrium states studied in Propositions 4 and 6.

9 The computations correspond to the reduced van der Waals EoS, with parameters
 10 (25). Cauchy problems for the system (53) are solved using a BDF method for
 11 stiff problems available in the Python ODE-solver package. The numerical results
 12 are computed for a large computational time $T_f = 200s$. For each test case, the
 13 state (τ, e) of the total system is picked either in the spinodal zone Z_{Spinodal} , in
 14 stable zones Z_{Stable} or in a metastable zones $Z_{\text{Metastable}}$, as depicted in Figure 2.
 15 We provide the associated vector field in the (α, φ, ξ) phase space and plot some
 16 trajectories in the phase space starting from arbitrary initial state $\mathbf{r}(0)$ in order to
 17 illustrate the attractivity of the equilibria. Several complementary trajectories are
 18 represented in the planes (τ, e) and (τ, p) .

19 **4.2.1. Spinodal zone.** The purpose is to illustrate the fact that, for any initial data
 20 $\mathbf{r}(0) \in]0, 1[^3$, if the state (τ, e) belongs to the spinodal zone Z_{Spinodal} , the correspond-
 21 ing attraction points are either \mathbf{r}^* or $\mathbf{r}^\#$, that is the system achieves a saturation
 22 state of the saturation dome, see Proposition 6.

23 We consider the state $(\tau, e) = (2, 2.5)$ belonging to the spinodal zone. The
 24 vector field of the dynamical system (53) is represented in Figure 3 by light blue
 25 arrows. For some random initial conditions $\mathbf{r}(0) \in]0, 1[^3$ (representing by green
 26 or yellow dots), the corresponding trajectories converge either towards the point
 27 $\mathbf{r}^* = (\alpha^*, \varphi^*, \xi^*)$ (green lines converging towards the green star) or towards $\mathbf{r}^\# =$
 28 $(1 - \alpha^*, 1 - \varphi^*, 1 - \xi^*)$ (yellow lines converging towards the yellow star). In both
 29 cases, the asymptotic state corresponds to the unique state (τ_i^*, e_i^*) , $i = 1, 2$, defined
 30 by (48), which belongs to the saturation dome, see Proposition 2-(2).

31 In Figures 4 and 5 are plotted trajectories corresponding to the initial condition

$$(59) \quad \mathbf{r}(0) = (0.2, 0.5, 0.42),$$

32 which corresponds to a state $(\tau_1(\mathbf{r}), e_1(\mathbf{r}))(0) = (0.8, 2.1)$ belonging to the sta-
 33 ble liquid zone with $p_1(0) = 0.2986$, $T_1(0) = 1.1166$ and $\mu_1(0) = 2.561$, and
 34 a state $(\tau_2(\mathbf{r}), e_2(\mathbf{r}))(0) = (3.2, 2.9)$ belonging to a metastable vapor state with
 35 $p_2(0) = 0.1006$, $T_2(0) = 1.0708$ and $\mu_2(0) = 2.2736$. Focusing on Figure 4-top,
 36 the trajectory $(\tau_1(\mathbf{r}), e_1(\mathbf{r}))(t)$ is represented with a dashed magenta line. One ob-
 37 serves that the trajectory starts from the magenta subcritical isothermal curve, goes
 38 through the stable liquid zone and converges towards a point of the saturation dome,
 39 see Figure 4-middle for a zoom of the trajectory. The trajectory $(\tau_2(\mathbf{r}), e_2(\mathbf{r}))(t)$
 40 (dashed orange line) is similar, except that it remains in the metastable vapor zone
 41 before converging towards a point of the saturation dome. The saturation asymp-
 42 totic state is characterized by the fractions

$$(60) \quad \mathbf{r}(T_f) = (0.255, 0.55, 0.47),$$

43 with $(\tau_1, e_1)(T_f) = (0.923, 2.15)$, $(\tau_2, e_2)(T_f) = (3.33, 2.93)$ and $p_1(T_f) = p_2(T_f) =$
 44 0.1 , $T_1(T_f) = T_2(T_f) = 1.077$, $\mu_1(T_f) = \mu_2(T_f) = 2.284$. See Figure 4-bottom for a

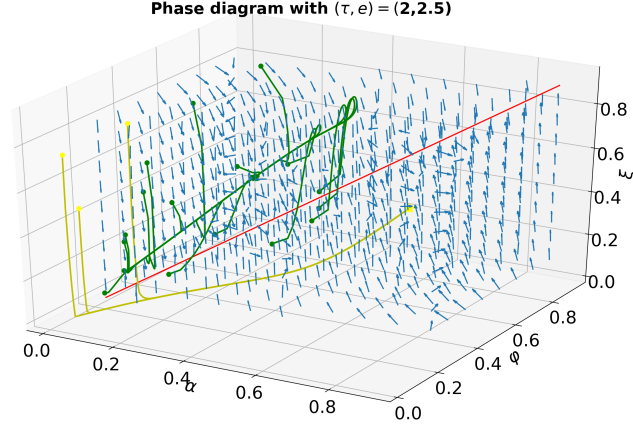


FIGURE 3. Spinodal zone: vector field of the dynamical system (53) (light blue arrows). The red line corresponds to the line $\alpha = \varphi = \xi$. Depending on the initial condition $\mathbf{r}(0)$, the trajectories converge either towards the equilibrium $\mathbf{r}^* = (\alpha^*, \varphi^*, \xi^*)$ (green lines) or towards $\mathbf{r}^\# = (1 - \alpha^*, 1 - \varphi^*, 1 - \xi^*)$ (yellow lines). In both case, the asymptotic regime corresponds to the state (τ_i^*, e_i^*) , $i = 1, 2$, defined by (48), belonging to the saturation dome.

1 zoom of the trajectory. Figures 5 represent the complementary trajectories plotted
2 in the (τ, p) plane.

3 4.2.2. *Stable phase zone.* The purpose is to illustrate the attraction of the line
4 $\alpha = \varphi = \xi$ for any initial data $\mathbf{r}(0) \in]0, 1[^3$, as soon as the state (τ, e) belongs
5 to a stable phase zone. The corresponding equilibrium is then the equilibrium
6 $(\tau_1(\bar{\mathbf{r}}), e_1(\bar{\mathbf{r}})) = (\tau_2(\bar{\mathbf{r}}), e_2(\bar{\mathbf{r}})) = (\tau, e)$, see Proposition 6.

7 We consider a state $(\tau, e) = (3, 3.1)$ belonging to the stable vapor zone. The
8 vector field of the dynamical system (53) is represented in Figure 6 by light blue
9 arrows. For some random initial conditions $\mathbf{r}(0) \in]0, 1[^3$ (represented by green dots),
10 the corresponding trajectories (green lines) converge towards points belonging to
11 the line $\alpha = \varphi = \xi$ plotted in red. Then the asymptotic states are such that
12 $(\tau_1(\bar{\mathbf{r}}), e_1(\bar{\mathbf{r}})) = (\tau_2(\bar{\mathbf{r}}), e_2(\bar{\mathbf{r}})) = (\tau, e)$.

13 In Figures 7 and 8 are plotted trajectories with the initial condition

$$(61) \quad \mathbf{r}(0) = (0.134, 0.5, 0.338),$$

14 which corresponds to a state $(\tau_1(\mathbf{r}), e_1(\mathbf{r}))(0) = (0.8, 2.1)$ belonging to the sta-
15 ble liquid zone, and a state $(\tau_2(\mathbf{r}), e_2(\mathbf{r}))(0) = (5.196, 4.1044)$ corresponding to a
16 supercritical state. Focusing on Figure 7, the trajectory $(\tau_1(\mathbf{r}), e_1(\mathbf{r}))(t)$ is repre-
17 sented with a dashed magenta line. One observes that it starts from the magenta
18 subcritical isothermal curve, goes over the critical point entering the supercritical
19 zone, and finally converges towards the point (τ, e) . The trajectory $(\tau_2(\mathbf{r}), e_2(\mathbf{r}))(t)$

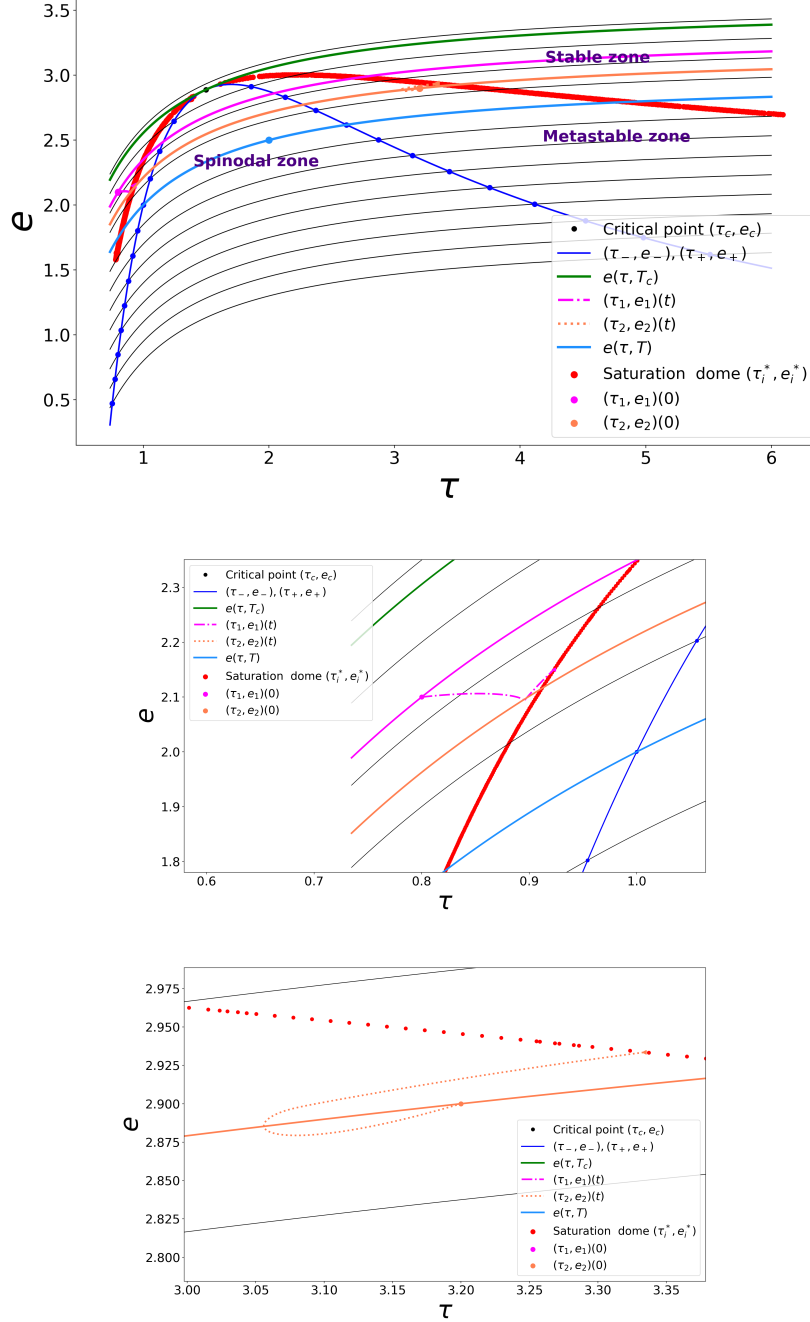


FIGURE 4. Spinodal zone, from top to bottom. Trajectories of the dynamical system (53) in the (τ, e) plane. Starting from an initial state $(\tau_1(\mathbf{r}), e_1(\mathbf{r}))(0)$ in the stable liquid region (on the magenta isothermal curve), the trajectory $(\tau_1(\mathbf{r}), e_1(\mathbf{r}))(t)$ is represented with a dashed magenta line and converges towards the saturation dome. The trajectory $(\tau_2(\mathbf{r}), e_2(\mathbf{r}))(t)$ is represented in orange. Middle and bottom figures: zoom of trajectories $(\tau_1(\mathbf{r}), e_1(\mathbf{r}))(t)$ and $(\tau_2(\mathbf{r}), e_2(\mathbf{r}))(t)$ respectively.

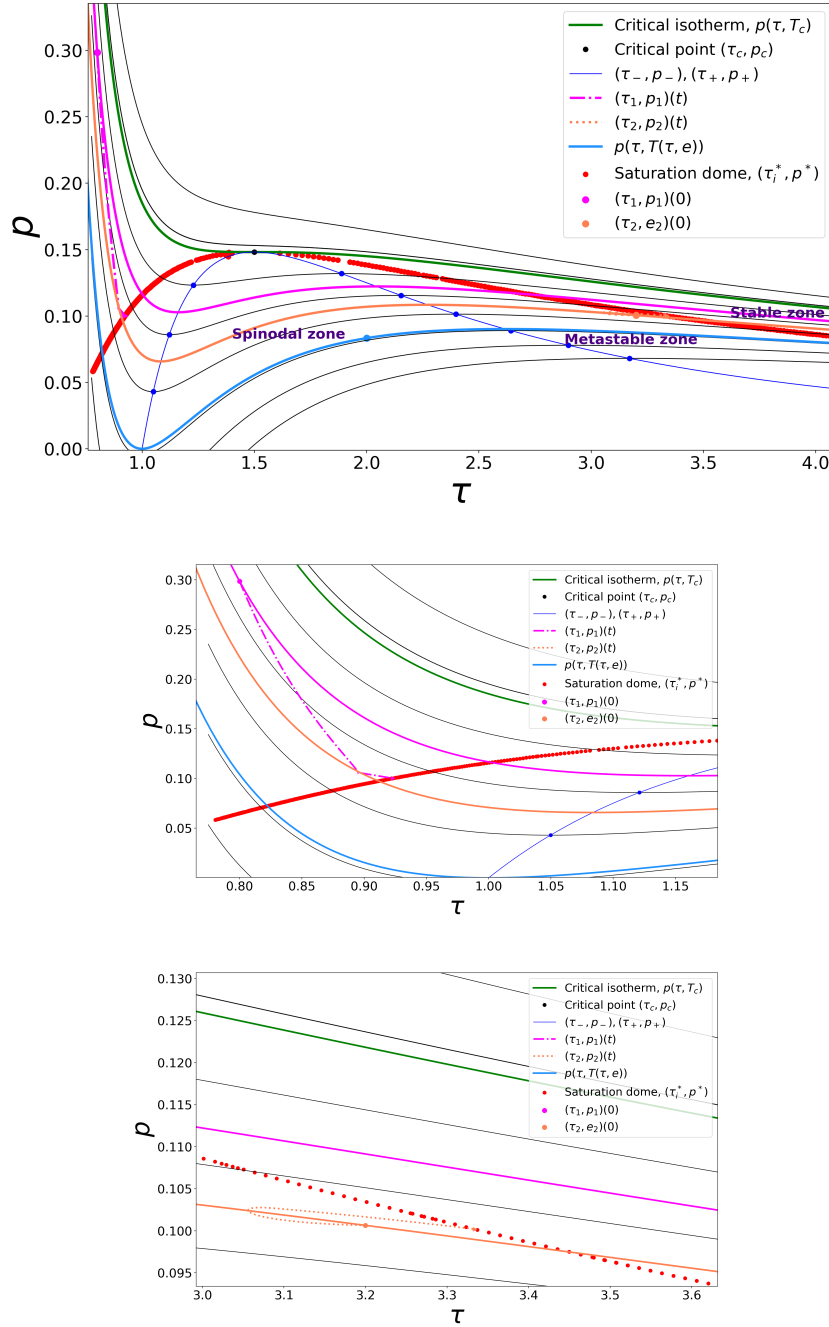


FIGURE 5. Spinodal zone, from top to bottom. Trajectories of the dynamical system (53) in the (τ, p) plane. Starting from an initial state $(\tau_1(\mathbf{r}), p(\tau_1(\mathbf{r}), e_1(\mathbf{r}))) (0)$ in the liquid region (on the isothermal curve in magenta), the trajectory $(\tau_1(\mathbf{r}), p(\tau_1(\mathbf{r}), e_1(\mathbf{r}))) (t)$ is represented with a dashed magenta line and converges towards the saturation dome. The trajectory $(\tau_2(\mathbf{r}), p(\tau_2(\mathbf{r}), e_2(\mathbf{r}))) (t)$ is represented in orange. Middle and bottom figures: zoom of trajectories $(\tau_1(\mathbf{r}), p(\tau_1(\mathbf{r}), e_1(\mathbf{r}))) (t)$ and $(\tau_2(\mathbf{r}), p(\tau_2(\mathbf{r}), e_2(\mathbf{r}))) (t)$ respectively.

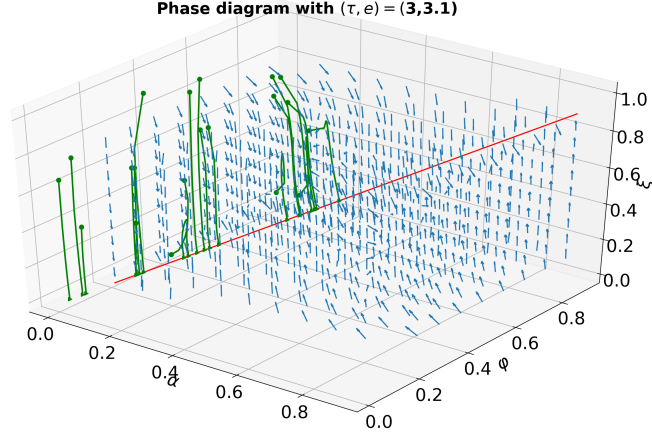


FIGURE 6. Stable phase zone: vector field of the dynamical system (53) (light blue arrows). The red line corresponds to the line $\alpha = \varphi = \xi$. For any initial condition $\mathbf{r}(0)$, the trajectories converge towards a point belonging to the line $\alpha = \varphi = \xi$, corresponding to the state (τ, e) .

1 (dashed orange line) is similar, going from the supercritical zone to the stable va-
 2 por zone and finally converging towards the point (τ, e) . Figure 8 represents the
 3 same trajectories plotted in the (τ, p) plane. One observes that the trajectory
 4 of $(\tau_1(\mathbf{r}), p(\tau_1(\mathbf{r}), e_1(\mathbf{r}))) (t)$ starts from the stable liquid zone, crosses the critical
 5 isothermal curve twice before converging towards the point $(\tau, p(\tau, e))$.

6 4.2.3. *Metastable zone.* The purpose is to illustrate the fact that, if the state (τ, e)
 7 belongs to a metastable zone, for any initial data $\mathbf{r}(0) \in]0, 1[^3$, there exist two
 8 possible attraction points.

9 We consider a state $(\tau, e) = (3.2, 2.5)$ belonging to the metastable vapor zone with
 10 $p(\tau, e) = 0.0759$ and $T(\tau, e) = 0.9375$. The vector field of the dynamical system (53)
 11 is represented in Figure 9 by light blue arrows. For some random initial conditions
 12 $\mathbf{r}(0) \in]0, 1[^3$ (represented by green or yellow dots), the complementary trajectories
 13 (green or yellow lines) converge towards

- either an attraction point which lies on the line $\alpha = \varphi = \xi$ (yellow trajec-
 tories). In that case the asymptotic state satisfies

$$(\tau_1(\bar{\mathbf{r}}), e_1(\bar{\mathbf{r}})) = (\tau_2(\bar{\mathbf{r}}), e_2(\bar{\mathbf{r}})) = (\tau, e),$$

14 and remains metastable, see Propositions 2-(1) and 4-(1);

- 15 • either the attraction point $\mathbf{r}^* = (\alpha^*, \varphi^*, \xi^*)$ (green trajectories) which con-
 16 cures with the unique state (τ_i^*, e_i^*) , $i = 1, 2$, defined by (48), which belongs
 17 to the saturation dome, see Propositions 2-(2) and 4-(2).

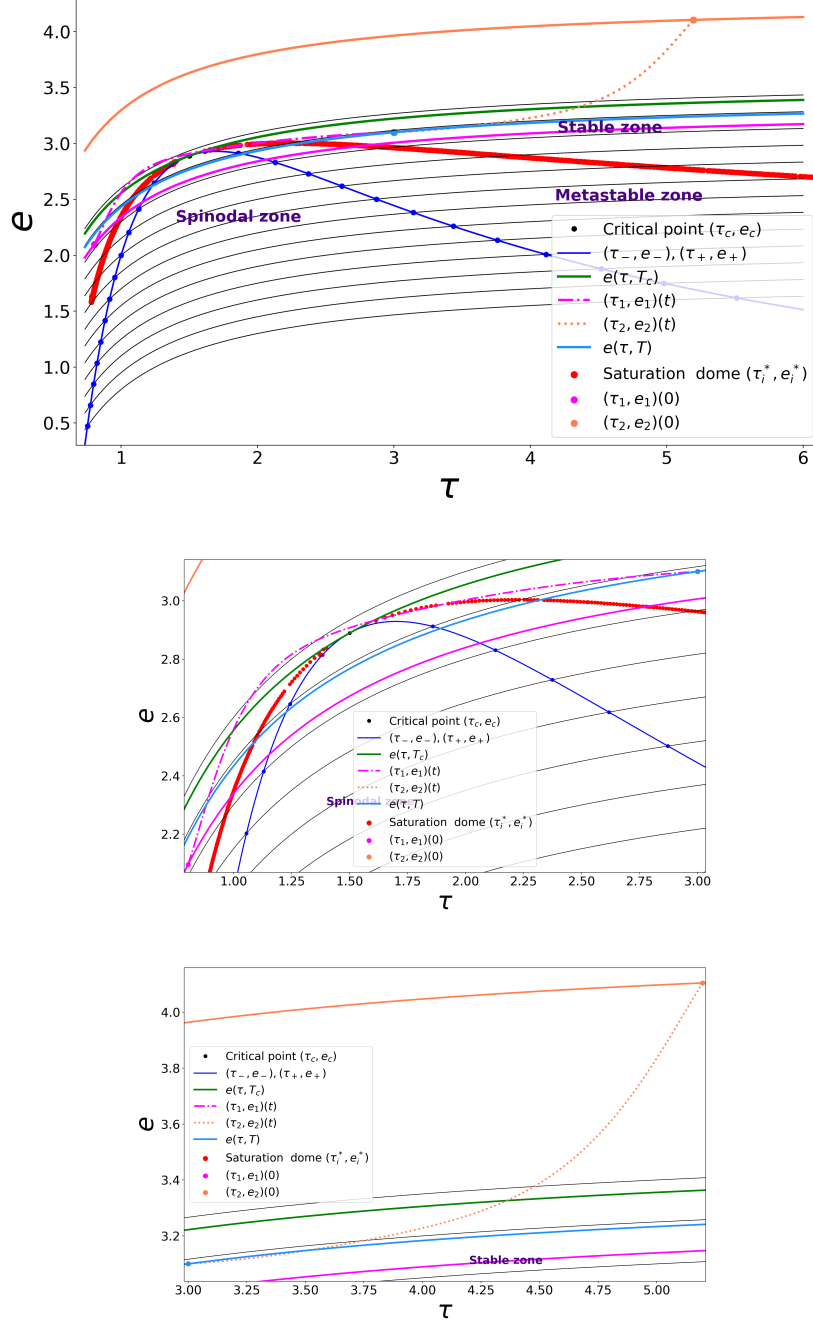


FIGURE 7. Stable phase zone. Trajectories of the dynamical system (53) in the (τ, e) plane. Starting from an initial state $(\tau_1(\mathbf{r}), e_1(\mathbf{r}))(0)$ in the stable liquid region (on the isothermal curve in magenta), the trajectory $(\tau_1(\mathbf{r}), e_1(\mathbf{r}))(t)$ is represented with a dashed magenta line and converges towards the state (τ, e) . The trajectory $(\tau_2(\mathbf{r}(t)), e_2(\mathbf{r}))(t)$ is represented in orange. Middle and bottom figures: zoom of trajectories $(\tau_1(\mathbf{r}), e_1(\mathbf{r}))(t)$ and $(\tau_2(\mathbf{r}), e_2(\mathbf{r}))(t)$ respectively.

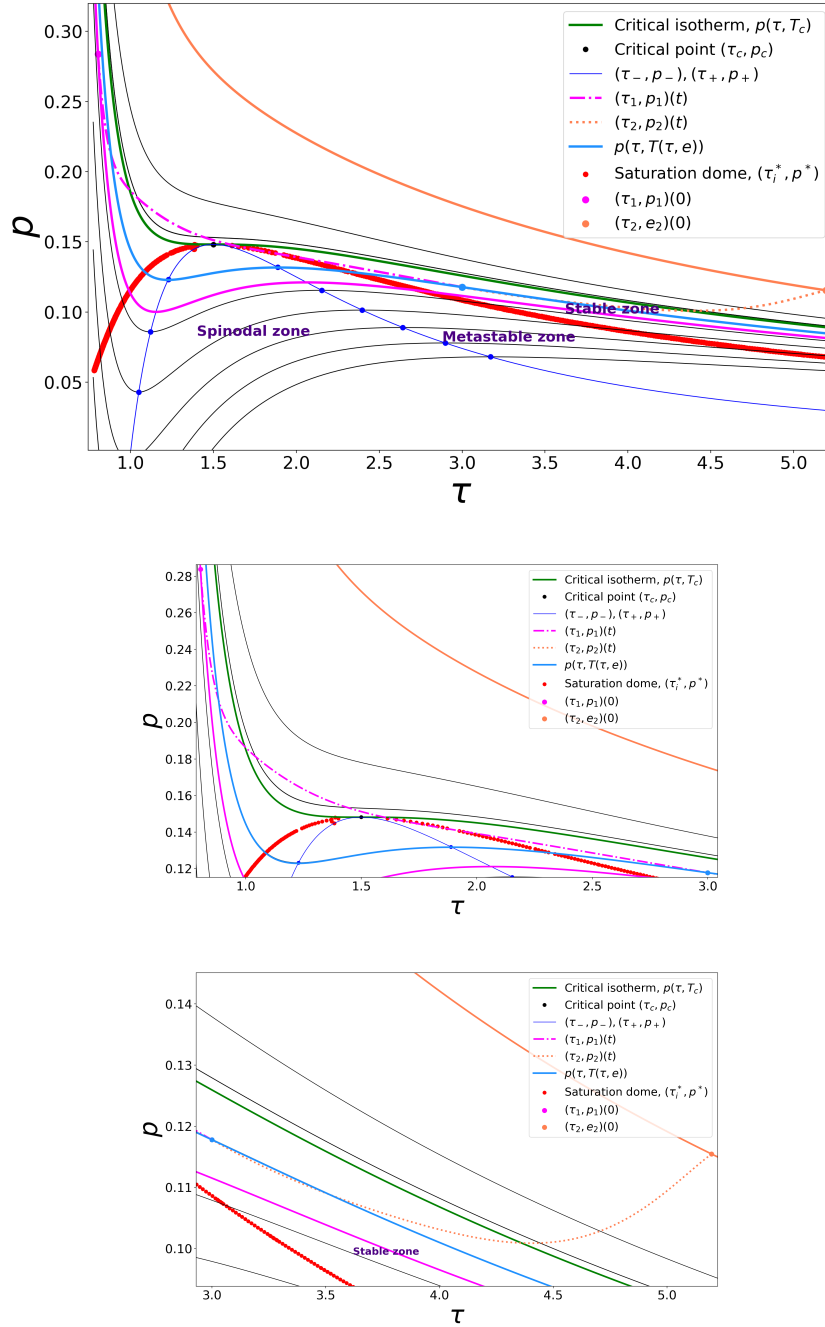


FIGURE 8. Stable phase zone, from top to bottom. Trajectories of the dynamical system (53) in the (τ, p) plane. Starting from an initial state $(\tau_1(\mathbf{r}), p(\tau_1(\mathbf{r}), e_1(\mathbf{r}))) (0)$ in the stable liquid region (on the isothermal curve in magenta), the trajectory $(\tau_1(\mathbf{r}), p(\tau_1(\mathbf{r}), e_1(\mathbf{r}))) (t)$ is represented with a dashed magenta line and converges towards the point (τ, e) . The trajectory $(\tau_2(\mathbf{r}), p(\tau_2(\mathbf{r}), e_2(\mathbf{r}))) (t)$ is represented in orange. Middle and bottom figures: zoom of trajectories $(\tau_1(\mathbf{r}), p(\tau_1(\mathbf{r}), e_1(\mathbf{r}))) (t)$ and $(\tau_2(\mathbf{r}), p(\tau_2(\mathbf{r}), e_2(\mathbf{r}))) (t)$ respectively.

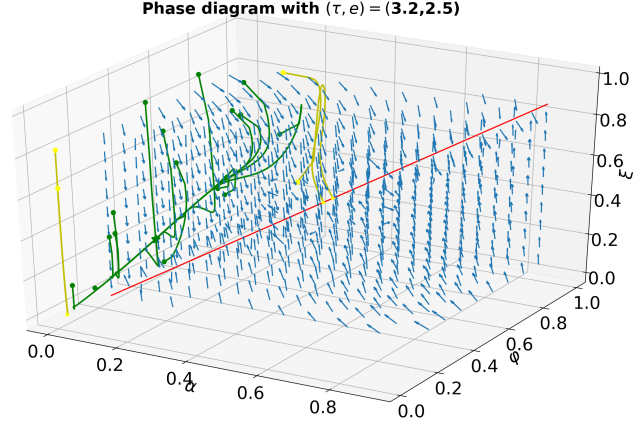


FIGURE 9. Metastable zone: vector field of the dynamical system (53) (light blue arrows). The red line corresponds to the line $\alpha = \varphi = \xi$. For any initial condition $\mathbf{r}(0)$, the trajectories converge either towards a point belonging to the line $\alpha = \varphi = \xi$, corresponding to the state (τ, e) (yellow trajectories), or to the point $\mathbf{r}^* = (\alpha^*, \varphi^*, \xi^*)$, which concurs with a state belonging to the saturation dome (green trajectories).

1 *Metastable state and perturbation within the phase.* In Figures 10 and 11 the
 2 represented trajectories correspond to a realization of the dynamical system for the
 3 initial condition

$$(62) \quad \mathbf{r}(0) = (0.5, 0.5, 0.55).$$

4 It boils down to an initial state $(\tau_1(\mathbf{r}), e_1(\mathbf{r}))(0) = (3.2, 2.75)$ in the metastable
 5 vapor zone with $p_1(0) = 0.091$, $T_1(0) = 1.02$, $\mu_1(0) = 2.15$, and to an initial state
 6 $(\tau_2(\mathbf{r}), e_2(\mathbf{r}))(0) = (3.2, 2.25)$ belonging to the spinodal zone with $p_2(0) = 0.06$,
 7 $T_2(0) = 0.85$, $\mu_2(0) = 1.75$. Notice that in this case, it holds $e_1(\mathbf{r})(0) > e > e_2(\mathbf{r})(0)$.
 8 The perturbation is small enough to ensure that the trajectories $(\tau_i(\mathbf{r}), e_i(\mathbf{r}))(t)$
 9 converge towards the point (τ, e) in the metastable zone. The asymptotic state is
 10 characterized by the fractions

$$(63) \quad \mathbf{r}(T_f) = (0.499, 0.499, 0.499),$$

11 with $p_1(T_f) = p_2(T_f) = 0.0759$ and $T_1(T_f) = T_2(T_f) = 0.9374$.

12 *Metastable state and perturbation outside the phase.* We provide in Figures 12
 13 and 13 the trajectories of the dynamical system for an initial condition

$$(64) \quad \mathbf{r}(0) = (0.16, 0.5, 0.328).$$

14 It corresponds to an initial state $(\tau_1(\mathbf{r}), e_1(\mathbf{r}))(0) = (0.8, 2.1)$ in the stable liq-
 15 uid zone and an initial state $(\tau_2(\mathbf{r}), e_2(\mathbf{r}))(0) = (5.376, 3.36)$ belonging to the sta-
 16 ble vapor zone. The perturbation is large enough to ensure that the trajectories
 17 $(\tau_i(\mathbf{r}), e_i(\mathbf{r}))(t)$ converge towards a state belonging to the saturation dome.

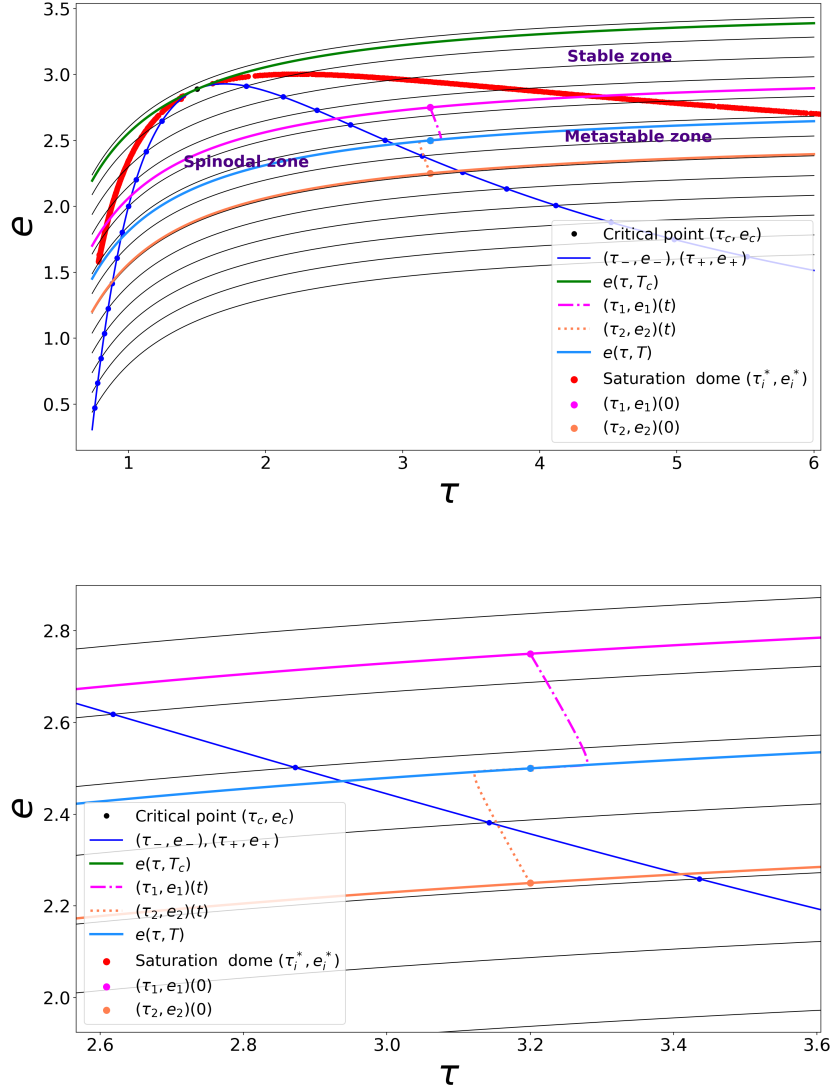


FIGURE 10. Metastable state and perturbation within the phase. Top figure: trajectories of the dynamical system (53) in the (τ, e) plane. Starting from an initial state $(\tau_1(\mathbf{r}), e_1(\mathbf{r}))(0)$ in the metastable vapor region (on the magenta isothermal curve), the trajectory $(\tau_1(\mathbf{r}), e_1(\mathbf{r}))(t)$ is represented with a dashed magenta line and converges towards the state (τ, e) . The trajectory $(\tau_2(\mathbf{r}), e_2(\mathbf{r}))(t)$ is represented in orange and starts with an initial condition in the spinodal zone. Bottom figure: zoom of trajectories $(\tau_i(\mathbf{r}), e_i(\mathbf{r}))(t)$.

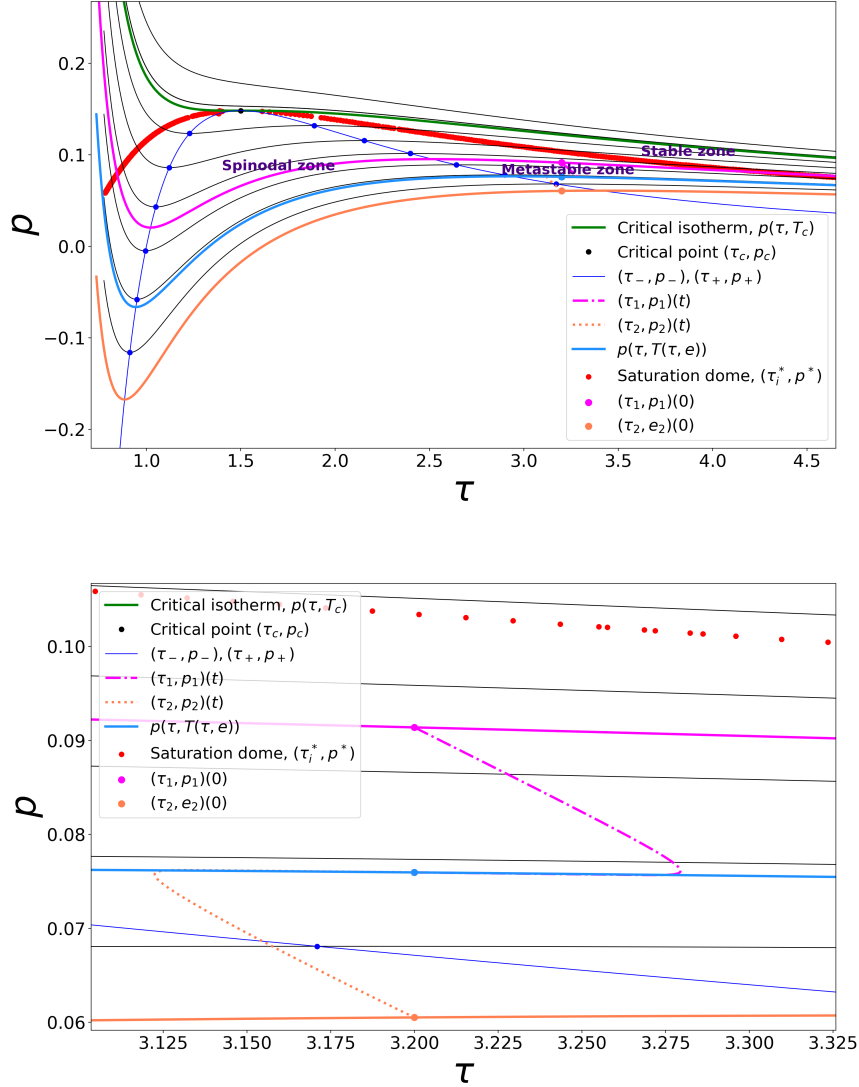


FIGURE 11. Metastable state and perturbation within the phase. Top figure: trajectories of the dynamical system (53) in the (τ, p) plane. Starting from an initial state $(\tau_1(\mathbf{r}), p(\tau_1(\mathbf{r}), e_1(\mathbf{r}))) (0)$ in the metastable vapor region (on the isothermal curve in magenta), the trajectory $(\tau_1(\mathbf{r}), p(\tau_1(\mathbf{r}), e_1(\mathbf{r}))) (t)$ is represented with a dashed magenta line and converges towards the point (τ, e) . The counterpart for the state $(\tau_2(\mathbf{r}), p(\tau_2(\mathbf{r}), e_2(\mathbf{r}))) (t)$ is represented in orange, and starts from an initial datum in the spinodal zone. Bottom figure: zoom of trajectories $(\tau_1(\mathbf{r}), p(\tau_1(\mathbf{r}), e_1(\mathbf{r}))) (t)$ and $(\tau_2(\mathbf{r}), p(\tau_2(\mathbf{r}), e_2(\mathbf{r}))) (t)$ respectively.

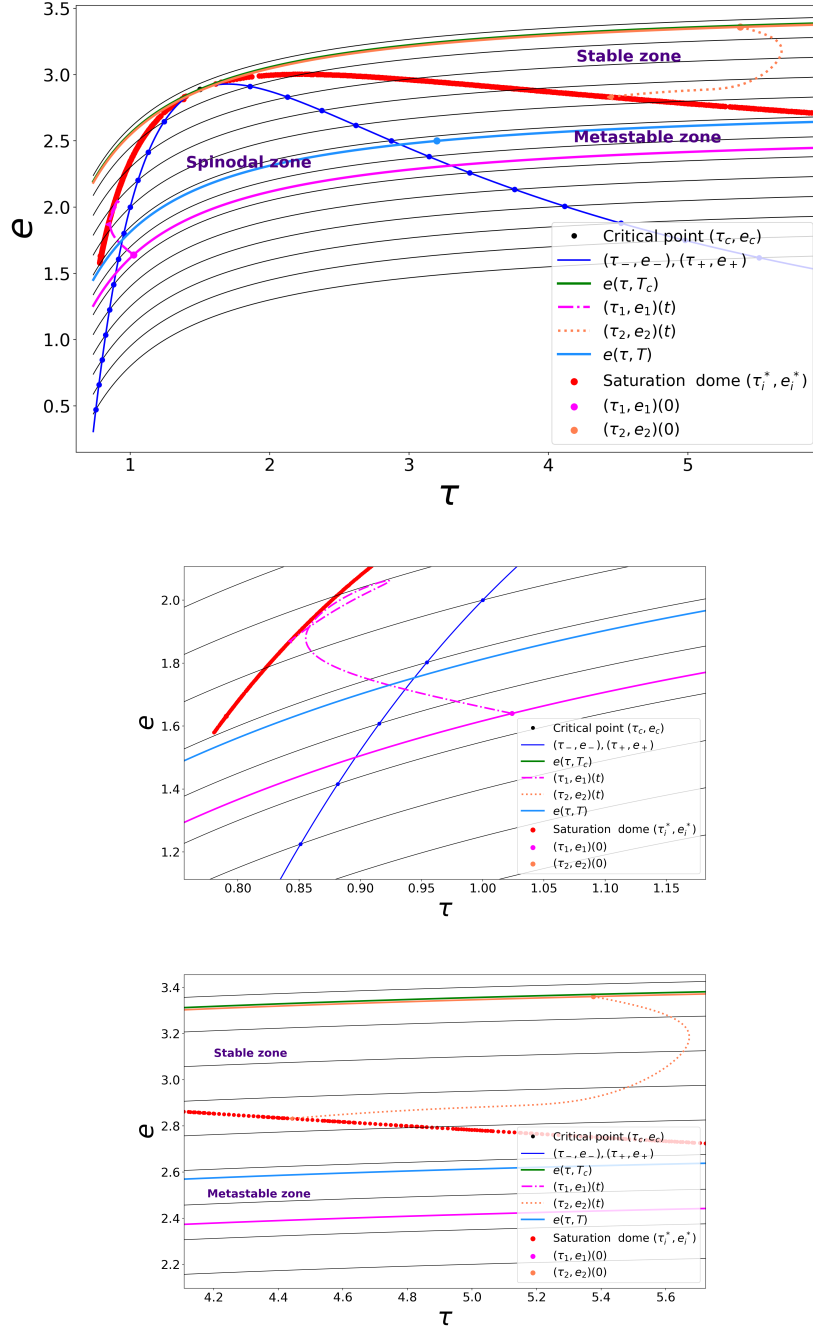


FIGURE 12. Metastable state and perturbation outside the phase. From top to bottom: trajectories of the dynamical system (53) in the (τ, e) plane. Starting from an initial state $(\tau_1(\mathbf{r}), e_1(\mathbf{r}))(0)$ in the metastable vapor region (on the magenta isothermal curve), the trajectory $(\tau_1(\mathbf{r}), e_1(\mathbf{r}))(t)$ is represented with a dashed magenta line and converges towards the state (τ, e) . The trajectory $(\tau_2(\mathbf{r}), e_2(\mathbf{r}))(t)$ is represented in orange and starts with an initial condition in the spinodal zone. Middle and bottom figures: zoom of trajectories $(\tau_i(\mathbf{r}), e_i(\mathbf{r}))(t)$.

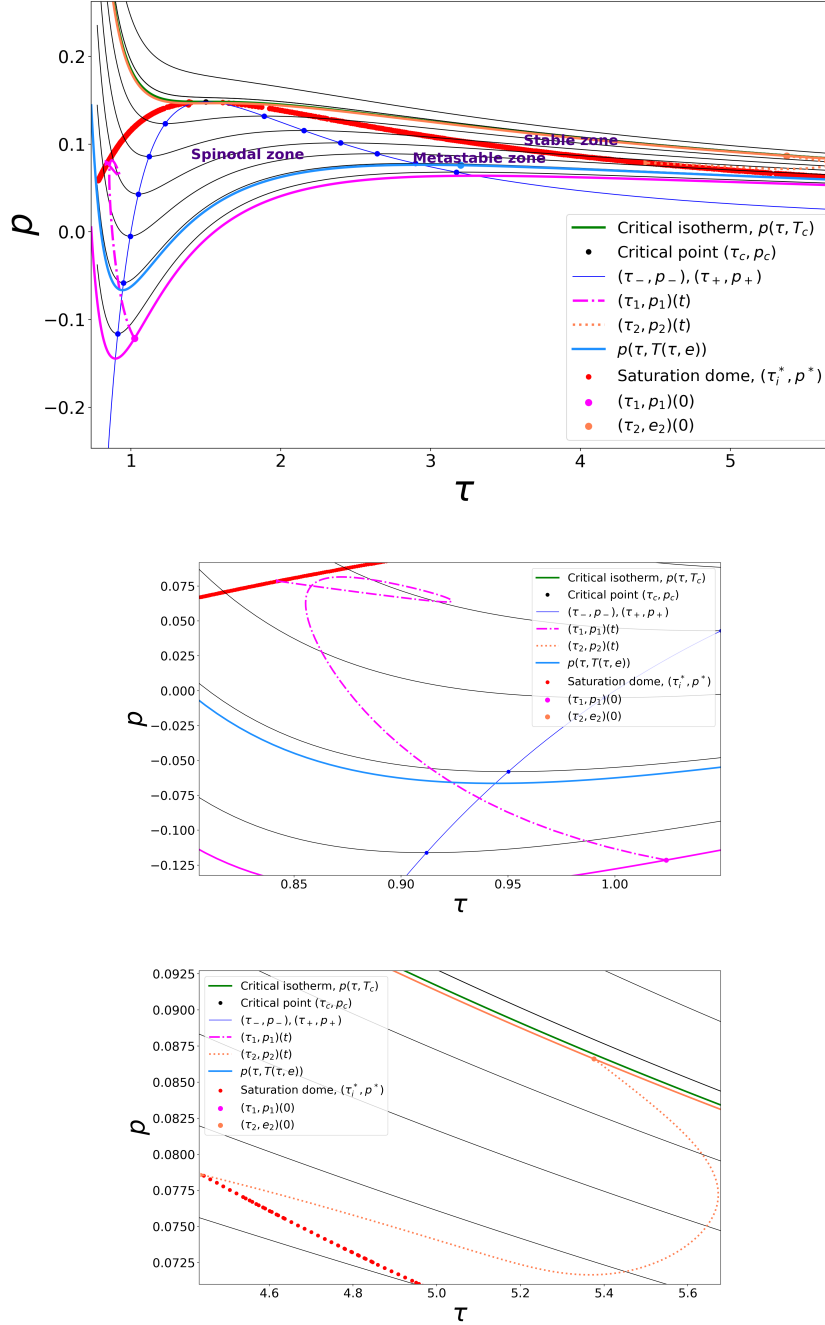


FIGURE 13. Metastable state and perturbation outside the phase. From top to bottom: trajectories of the dynamical system (53) in the (τ, p) plane. Starting from an initial state $(\tau_1(\mathbf{r}), p(\tau_1(\mathbf{r}), e_1(\mathbf{r}))) (0)$ in the stable liquid region (on the magenta isothermal curve), the trajectory $(\tau_1(\mathbf{r}), p(\tau_1(\mathbf{r}), e_1(\mathbf{r}))) (t)$ is represented with a dashed magenta line and converges towards the point (τ, e) . The trajectory $(\tau_2(\mathbf{r}), p(\tau_2(\mathbf{r}), e_2(\mathbf{r}))) (t)$ is represented in orange. Middle and bottom figures: zoom of trajectories $(\tau_1(\mathbf{r}), p(\tau_1(\mathbf{r}), e_1(\mathbf{r}))) (t)$ and $(\tau_2(\mathbf{r}), p(\tau_2(\mathbf{r}), e_2(\mathbf{r}))) (t)$ respectively.

1 5. A HOMOGENEOUS RELAXATION MODEL

2 The aim of this Section is to investigate the impact of the fluid dynamics on the
 3 stability of metastable states and the apparition of phase transition. To do so we
 4 now consider the liquid-vapor mixture as a compressible medium. It is described
 5 by its density $\rho(t, x)$ (and $\tau(t, x) = 1/\rho(t, x)$ its specific volume), its velocity $u(t, x)$
 6 and its internal energy $e(t, x)$, depending on the time variable $t \in \mathbb{R}^+$ and the one-
 7 dimensional space variable $x \in \mathbb{R}$. Since both phases evolve with the same velocity
 8 u , we focus on so-called homogeneous models in the spirit of [3, 22].

9 The homogeneous model reads

$$(65) \quad \begin{cases} \partial_t(\rho\alpha) + \partial_x(\rho u\alpha) = \frac{\rho}{\varepsilon} \mathbb{F}^\alpha(\mathbf{r}), \\ \partial_t(\rho\varphi) + \partial_x(\rho u\varphi) = \frac{\rho}{\varepsilon} \mathbb{F}^\varphi(\mathbf{r}), \\ \partial_t(\rho\xi) + \partial_x(\rho u\xi) = \frac{\rho}{\varepsilon} \mathbb{F}^\xi(\mathbf{r}), \\ \partial_t(\rho) + \partial_x(\rho u) = 0, \\ \partial_t(\rho u) + \partial_x(\rho u^2 + p) = 0, \\ \partial_t(\rho E) + \partial_x(\rho u E + up) = 0, \end{cases}$$

10 where $E = e + u^2/2$ is the total energy. The last three equations correspond to
 11 the Euler's system with a mixture pressure law p to be define in the sequel. The
 12 first three equations are evolution equations of the fractions $\mathbf{r} = (\alpha, \varphi, \xi) \in]0, 1[^3$,
 13 with relaxation source terms $(\mathbb{F}^\alpha, \mathbb{F}^\varphi, \mathbb{F}^\xi)$ towards the Thermodynamic equilibrium,
 14 which coincide with the dynamical system (53) studied in the previous section.
 15 The parameter $\varepsilon > 0$ stands for a relaxation time towards the thermodynamic
 16 equilibrium.

17

Remark 3. We have chosen to use the same relaxation time-scale for the three
 relaxation terms. This choice might be non physical according to few references.
 In [13] the author provides an estimate of the mechanical time relaxation in a two-
 phase flow. In [25] the authors consider a two-velocity model and order the thermal
 time-scale λ_T , the mechanical relaxation time scale λ_p and the kinetic relaxation
 time-scale λ_u as follows

$$0 < \lambda_p, \lambda_u \ll \lambda_T.$$

18 Hence one should consider at least another relaxation time in the equation on the
 19 energy fractions. We choose to consider the same time-scale for all the relaxation
 20 processes rather than impose an arbitrary choice of different time-scales. One must
 21 be aware that this choice may lead to stiff problems and numerical difficulties.

22 **5.1. Properties of the homogeneous relaxation model.** First, we focus on the
 23 convective part of the model (65). It consists in the Euler system complemented
 24 with convection equations of the fractions $\mathbf{r}(t, x)$; thus it inherits from the wave
 25 structure of the Euler system. In order to close the system, in agreement with
 26 the thermodynamical constraints presented in the previous sections, the considered
 27 pressure p is a function of the density ρ , the internal energy e and the fraction
 28 vector \mathbf{r} . Following [3, 21, 18, 22], the mixture pressure law should be derived from
 29 the mixture entropy function \mathcal{S} defined in (51).

30 Highlighting the dependency on (τ, e) , the entropy of the mixture reads

$$(66) \quad \mathcal{S}(\tau, e, \mathbf{r}) = \varphi s(\tau_1(\mathbf{r}), e_1(\mathbf{r})) + (1 - \varphi) s(\tau_2(\mathbf{r}), e_2(\mathbf{r})),$$

1 where s is again the van der Waals EoS and the functions $\tau_i(\mathbf{r})$ and $e_i(\mathbf{r})$ are defined
 2 in (50). The associated pressure p and the temperature T of the mixture are deduced
 3 from an extended Gibbs relation

$$(67) \quad Td\mathcal{S}(\tau, e, \mathbf{r}) = de + pd\tau + \frac{\partial\mathcal{S}}{\partial\alpha}d\alpha + \frac{\partial\mathcal{S}}{\partial\varphi}d\varphi + \frac{\partial\mathcal{S}}{\partial\xi}d\xi.$$

4 Then the definitions of the mixture temperature and pressure, as functions of
 5 (τ, e, \mathbf{r}) , are

$$(68) \quad \begin{aligned} \frac{1}{T(\tau, e, \mathbf{r})} &= \frac{\xi}{T(\tau_1(\mathbf{r}), e_1(\mathbf{r}))} + \frac{1-\xi}{T(\tau_2(\mathbf{r}), e_2(\mathbf{r}))}, \\ \frac{p(\tau, e, \mathbf{r})}{T(\tau, e, \mathbf{r})} &= \alpha \frac{p(\tau_1(\mathbf{r}), e_1(\mathbf{r}))}{T(\tau_1(\mathbf{r}), e_1(\mathbf{r}))} + (1-\alpha) \frac{p(\tau_2(\mathbf{r}), e_2(\mathbf{r}))}{T(\tau_2(\mathbf{r}), e_2(\mathbf{r}))}. \end{aligned}$$

6 The sound speed of the system (65) is

$$(69) \quad c^2 = -\tau^2 \frac{\partial}{\partial\tau} p + \tau^2 p \frac{\partial}{\partial e} p,$$

7 which, using the expression of the mixture pressure (68), simplifies to

$$(70) \quad \begin{aligned} -\frac{c^2}{T\tau^2} &= \frac{1}{\varphi}(-\alpha, \xi p) Hs_1 \begin{pmatrix} -\alpha \\ \xi p \end{pmatrix} \\ &+ \frac{1}{1-\varphi}(-(1-\alpha), (1-\xi)p) Hs_2 \begin{pmatrix} -(1-\alpha) \\ (1-\xi)p \end{pmatrix}, \end{aligned}$$

8 where Hs_i denotes the hessian matrix of the phasic entropy s at (τ_i, e_i)

$$(71) \quad Hs_i(\tau_i, e_i) = \begin{pmatrix} \frac{\partial^2 s}{\partial\tau_i^2}(\tau_i, e_i) & \frac{\partial^2 s}{\partial\tau_i\partial e_i}(\tau_i, e_i) \\ \frac{\partial^2 s}{\partial e_i\partial\tau_i}(\tau_i, e_i) & \frac{\partial^2 s}{\partial e_i^2}(\tau_i, e_i) \end{pmatrix},$$

9 and the dependency to the variables has been skipped for readability reasons.

10 The convective system is hyperbolic if and only if the right-hand side of (70)
 11 is negative. This is the case if the hessian matrices Hs_1 and Hs_2 are negative
 12 definite, which is true in concavity region of the van der Waals entropy, that is
 13 outside the spinodal region Z_{Spinodal} . Hence the system is non-strictly hyperbolic.
 14 However, it has been highlighted in [24] in the isothermal context that the domains
 15 of hyperbolicity of (65) strongly depend on the attraction basins of the dynamical
 16 system (53). More precisely, the invariant domains of hyperbolicity for the relaxed
 17 system are subsets of the attraction basins of the dynamical system.

18 The convective part of the model (65) inherits the wave structure of the Euler
 19 system. The fields associated with the fractions \mathbf{r} are linearly degenerated with
 20 the eigenvalue u and the mass equation is linearly degenerated with velocity u .
 21 The momentum and energy conservation laws are genuinely nonlinear fields with
 22 velocities $u \pm c$ because the system inherits from the Euler system with a complex
 23 EoS. Hence one can mimic the proof given in [17] for instance. But, the proof holds
 24 true only in the concavity region of the mixture entropy (66), that is to say in
 25 the region of strict hyperbolicity. The Riemann invariants associated to the wave
 26 of velocity u are the velocity u and the pressure. Moreover the volume fraction,
 27 the mass fraction and the energy fraction are Riemann invariants associated to the
 28 genuinely nonlinear waves. The positivity of the fractions is ensured by both the
 29 positivity property of the dynamical system, see Proposition 3-(1), and the form of
 30 the convection equations of the fractions \mathbf{r} , see [23].

1 **5.2. Numerical illustrations.** Numerous numerical schemes have been proposed
 2 for homogeneous models with relaxation, see again [3] and [22] for models involving
 3 stiffened gas or tabulated laws. We propose here a very standard approach, and
 4 take a special interest to numerical illustrations.

5 The numerical approximation consists in a fractional step method.

6 We restrict to regular meshes of size $\Delta x = x_{i+\frac{1}{2}} - x_{i-\frac{1}{2}}$, $i \in \mathbb{Z}$. The time step
 7 is $\Delta t = t^{n+1} - t^n$, $n \in \mathbb{N}$. We focus on the convective part of (65) with an initial
 8 condition

$$(72) \quad \begin{cases} \partial_t W + \partial_x F(W) = 0, \\ W(0, x) = W_0(x), \end{cases}$$

9 with $W = (\rho\alpha, \rho\varphi, \rho\xi, \rho, \rho u, \rho E)^T$, and $F(W) = uW + pD$, with $D = (0, 0, 0, 0, 1, u)^T$.
 10 Let $W(t^n, x)$ be approximated by

$$(73) \quad W_i^n = \frac{1}{\Delta x} \int_{x_{i-\frac{1}{2}}}^{x_{i+\frac{1}{2}}} W(t^n, x) dx.$$

11 Integrating the system (72) on the space-time domain $[x_{i-\frac{1}{2}}, x_{i+\frac{1}{2}}] \times [t^n, t^{n+1,*}]$
 12 provides

$$(74) \quad \begin{aligned} & \int_{x_{i-\frac{1}{2}}}^{x_{i+\frac{1}{2}}} (W(t^{n+1,*}, x) - W(t^n, x)) dx \\ & + \int_{t^n}^{t^{n+1,*}} (F(W(t, x_{i+\frac{1}{2}})) - F(W(t, x_{i-\frac{1}{2}}))) dt = 0. \end{aligned}$$

13 Using the notation (73), one obtains

$$(75) \quad W_i^{n+1,*} = W_i^n - \frac{\Delta t}{\Delta x} \left(\mathcal{F}_{i+\frac{1}{2}}^n - \mathcal{F}_{i-\frac{1}{2}}^n \right),$$

14 where $\int_{t^n}^{t^{n+1,*}} F(W(t, x_{i+\frac{1}{2}})) dt$ is approximated by an explicit numerical flux clas-
 15 sically involving the two neighboring cells of interface $x_{i+\frac{1}{2}}$: $\mathcal{F}_{i+\frac{1}{2}}^n = F(W_i^n, W_{i+1}^n)$

16 In the following, we choose the explicit HLLC numerical flux [34] to define the
 17 fluxes $\mathcal{F}_{i+1/2}^n$ through the interface $x_{i+1/2}$.

18 The source terms of the system (65) are accounted for discretizing

$$(76) \quad \begin{cases} \frac{d}{dt} \rho(t) = 0, & \frac{d}{dt} (\rho\alpha)(t) = \frac{\rho}{\varepsilon} \mathbb{F}_\alpha(\mathbf{r}, \rho, e), \\ \frac{d}{dt} (\rho u)(t) = 0, & \frac{d}{dt} (\rho\varphi)(t) = \frac{\rho}{\varepsilon} \mathbb{F}_\varphi(\mathbf{r}, \rho, e), \\ \frac{d}{dt} (\rho E)(t) = 0, & \frac{d}{dt} (\rho\xi)(t) = \frac{\rho}{\varepsilon} \mathbb{F}_\xi(\mathbf{r}, \rho, e). \end{cases}$$

19 It can be written in an equivalent manner

$$(77) \quad \begin{cases} \frac{d}{dt} \alpha(t) = \frac{1}{\varepsilon} \mathbb{F}_\alpha(\mathbf{r}(t), \rho(0), e(0)), \\ \frac{d}{dt} \varphi(t) = \frac{1}{\varepsilon} \mathbb{F}_\varphi(\mathbf{r}(t), \rho(0), e(0)), \\ \frac{d}{dt} \xi(t) = \frac{1}{\varepsilon} \mathbb{F}_\xi(\mathbf{r}(t), \rho(0), e(0)). \end{cases}$$

20 The numerical approximation W^{n+1} is an approximated solution of the system (76)
 21 at time $t = \Delta t$ with the initial condition $W^{n+1,*}$ deduced from the convection step.

1 The numerical method for the convective part has been validated on diphasic
 2 test cases with a real van der Waals EoS proposed in [12]. Our HLLC results
 3 are comparable to the results given by the Rusanov scheme. Nonetheless these two
 4 numerical schemes are not robust enough to solve properly the contact discontinuity.
 5 This inaccuracy is related to the difficulty in conservative methods for Euler-like
 6 models with nonlinear equation of state. More accurate results may have been
 7 obtained using the VFRoe-ncv or VFFC schemes defined in [12] or adaptive schemes
 8 like in [27].

9 In order to capture accurately the thermodynamic equilibrium, one should ideally
 10 consider infinitely fast relaxation with $\varepsilon = 0$. The integration of the source terms
 11 (77) reduces the projection of the solution on the appropriate equilibrium (described
 12 in Proposition 4), depending on the basin of attraction that state $W^{n+1,*}$ belongs
 13 to.

14 Unfortunately, as mentioned in Section 4.1, the boundaries of the basins of at-
 15 traction are not explicitly defined. This is for instance the case of the basins of
 16 attraction of the spinodal zone and the metastable zones. These basins are either
 17 delimited by the saturation dome, which determination requires the resolution of
 18 the nonlinear system (48), or by an unstable manifold, which numerical approxi-
 19 mation is intrinsically not reachable. Hence, we consider in the sequel finite but
 20 sufficiently small relaxation time parameter ε coupled with a Runge-Kutta 4 inte-
 21 gration method.

22 The following numerical results are solely illustrations of the homogeneous relax-
 23 ation model behaviour. The development of more appropriate numerical strategies
 24 is beyond the scope of the present work.

25 5.2.1. *Stable diphasic test case.* We provide a validation test case which mimics
 26 the one proposed in [12], for a non-reduced van der Waals equation of state. The
 27 Riemann data correspond to a left stable liquid state, see the magenta dot in Figure
 28 14 and a right stable vapor state, see the coral dot in Figure 14, namely

$$(78) \quad \begin{aligned} \rho_L = 1.111, \quad u_L = 0, \quad p_L = 0.2, \quad \alpha_L = \varphi_L = \xi_L = 10^{-6}, \\ \rho_R = 0.277, \quad u_R = 0, \quad p_R = 0.11 \quad \alpha_R = \varphi_R = \xi_R = 10^{-6}. \end{aligned}$$

29 This test case corresponds to a single-phase subsonic 1-rarefaction wave, since
 30 the fractions are constant and small. The domain $[0, 1]$ is decomposed into 1000
 31 cells and the discontinuity is applied at $x_0 = 0.5$. The final time of computation is
 32 0.4 and the CFL coefficient is 0.9.

33 The global behaviour given in Figure 15 is consistent with the results provided
 34 in [12]. In particular, the curve profiles around the contact discontinuity is not
 35 precise enough. A more robust numerical flux should be considered to overcome the
 36 problem, which actually disappears as the grid is refined. Note that the undershoots
 37 remain in the pressure and velocity profiles when refining the grid, even though their
 38 amplitude decrease. The fractions are not plotted since they are constant in space
 39 and equal to 10^{-6} .

40 5.2.2. *Weak acoustic perturbation of a metastable vapor state.* This example con-
 41 sists in a constant metastable vapor state submitted to a weak compression. A
 42 similar test case has been studied in [15] in the isothermal case. The initial state is

$$(79) \quad \rho = 0.3125, \quad p = 0.09, \quad \alpha = 0.16, \quad \varphi = 0.5, \quad \xi = 0.3285,$$

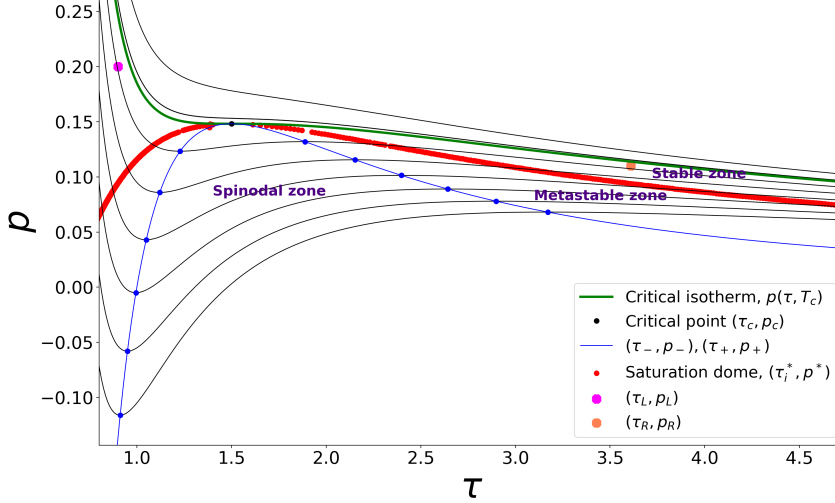


FIGURE 14. Initial data for the stable diphasic test in plane (τ, p) .

1 which corresponds to the magenta dot in Figure 16. We impose a small compression
 2 from the left with velocity $u_L = 0.1$, while $u_R = 0$. The domain $[0, 1]$ is discretized
 3 with 1000 cells, and the solution is computed at time 0.1, with a CFL number 0.9.
 4 In Figure 17, one observes the appearance of a droplet around $x = 0.5$. In the
 5 droplet, the density reaches a saturation value which corresponds to the coral state
 6 (τ_*, p_*) plotted in Figure 16. Indeed, the fractions are different but the pressures
 7 p_i , the temperatures T_i and the chemical potential μ_i (which are not plotted here)
 8 are equal.

9 5.2.3. *Strong acoustic perturbation of a metastable vapor state.* In this case, we keep
 10 the same initial data as in the previous one but we impose a stronger compression
 11 from the left with velocity $u_L = 0.9$. A similar test case is provided in [15] in
 12 the isothermal case. The domain $[0, 1]$ is also discretized with 1000 cells, and the
 13 solution is computed at time 0.1, with a CFL number 0.9. Here, the strong compression
 14 induces the appearance of a droplet which moves from the left to the right,
 15 see Figure 19. One observes not only that the pressures p_i , the temperatures T_i and
 16 the chemical potentials μ_i (which are not plotted here) are equal but also that the
 17 fractions are equal inside the droplet. Hence only one phase remains in the droplet.
 18 Concentrating on the density and pressure values inside the droplet, one observes
 19 that it coincides with a supercritical state (τ_*, p_*) , represented by a coral dot in
 20 Figure 18.

21

6. CONCLUSION

22 This paper concerns the construction of appropriate relaxation source terms to-
 23 wards thermodynamic equilibrium for a liquid-vapor flow with the possible appear-
 24 ance of metastable states. Extending the works [24, 15] in the isothermal context,
 25 the two phases are assumed to follow the same non convex van der Waals equation
 26 of state. We provide time evolution equations of the fractions of volume, mass and

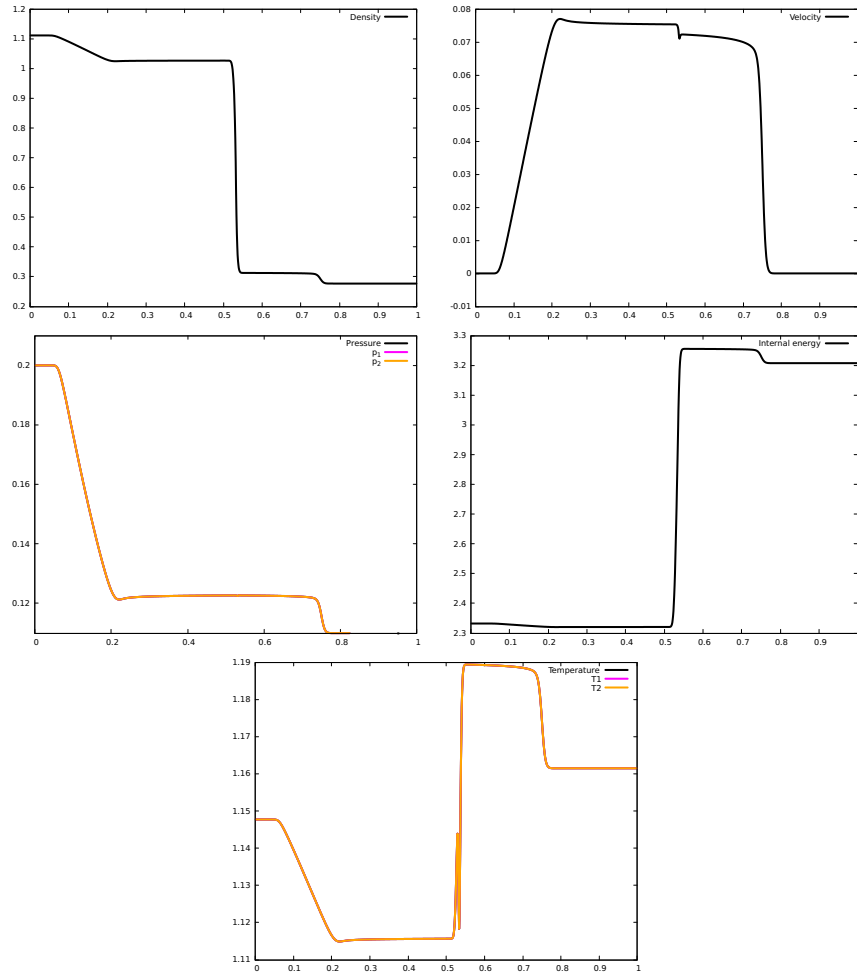


FIGURE 15. Stable diphasic test. From top left to bottom right: density profile, velocity, pressure, internal energy and temperature profile with respect to the space variable.

1 energy of one of the phases which guarantee the growth of the mixture entropy.
 2 The dynamical model admits three major properties. First the attractive equilibria
 3 are either saturation states, characterized by the equalities of the phasic pressures,
 4 temperatures and chemical potentials, or stable or metastable states, for which the
 5 two phases coincide. In the latter case, the equilibrium states correspond to the
 6 equality of the fractions to some asymptotic value strictly between 0 and 1. The
 7 fluid is either in a liquid or vapor, metastable or stable, state, but the fractions do
 8 not cancel, in contrast with the classical Baer-Nunziato type models. Second, when
 9 considering a mixture state belonging to a metastable zone, there are two possi-
 10 ble equilibria depending the initial condition on the fractions. The system either
 11 reaches a saturation state or converges towards the metastable initial state charac-
 12 terized by the identification of the two phases. Third, the systems allow to deal with
 13 supercritical cases as well. The method we propose here could be extended to more

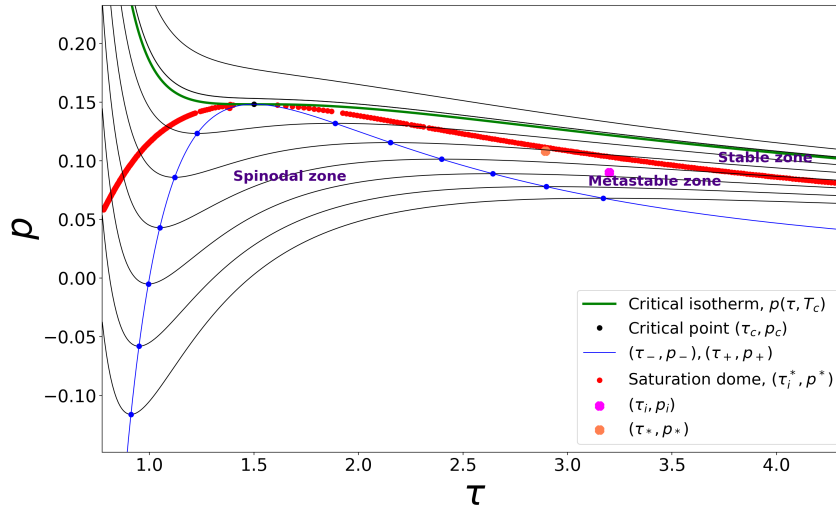


FIGURE 16. Initial (τ_i, e_i) and intermediate (τ_*, e_*) data for a weak acoustic perturbation of a metastable vapor state in the plane (τ, p) .

1 realistic non convex cubic equations of state as considering Soave-Redlich-Kwong
 2 [33] or the Peng-Robinson [29] models. Using tabulated laws could be a real issue
 3 because of the difficulty of determining the attraction basins. Another issue is the
 4 coupling with fluid dynamics, which is merely illustrated here. It deserves a more
 5 careful study, from both theoretical and numerical viewpoints.

6 ACKNOWLEDGMENTS

7 Hala Ghazi and H el ene Mathis would like to thank the Centre Henri Lebesgue
 8 ANR-11-LABX-0020-01 for its support.

9 REFERENCES

- 10 [1] M. R. Baer and J. W. Nunziato. A two phase mixture theory for the deflagration to detonation
 11 (ddt) transition in reactive granular materials. *Int. J. Multiphase Flow*, 12(6):861–889, 1986.
 12 [2] D. W. Ball. Physical Chemistry. *Cengage Learning*, 2002., 2011.
 13 [3] [10.1016/j.compfluid.2004.06.004] T. Barberon and P. Helluy. Finite volume simulation of
 14 cavitating flows. *Computers and Fluids*, 34(7):832–858, 2005.
 15 [4] J. Bartak. A study of the rapid depressurization of hot water and the dynamics of vapour
 16 bubble generation in superheated water. *Int. J. Multiph. Flow*, 16(5):789–98, 1990.
 17 [5] H. B. Callen. Thermodynamics and an introduction to thermostatistics, second edition. *Wiley
 18 and Sons*, 1985.
 19 [6] F. Caro. *Mod elisation et simulation num erique des transitions de phase liquide vapeur*. PhD
 20 thesis, Ecole Polytechnique X, 2004.
 21 [7] M. De Lorenzo. *Modelling and numerical simulation of metastable two-phase flows*. PhD
 22 thesis, Universit e Paris-Saclay , May 2018.
 23 [8] M. De Lorenzo, Ph. Lafon, M. Di Matteo, M. Pelanti, J.-M. Seynhaeve, and Y. Bartosiewicz.
 24 Homogeneous two-phase flow models and accurate steam-water table look-up method for fast
 25 transient simulations. *Int. J. Multiph. Flow*, 95:199–219, 2017.

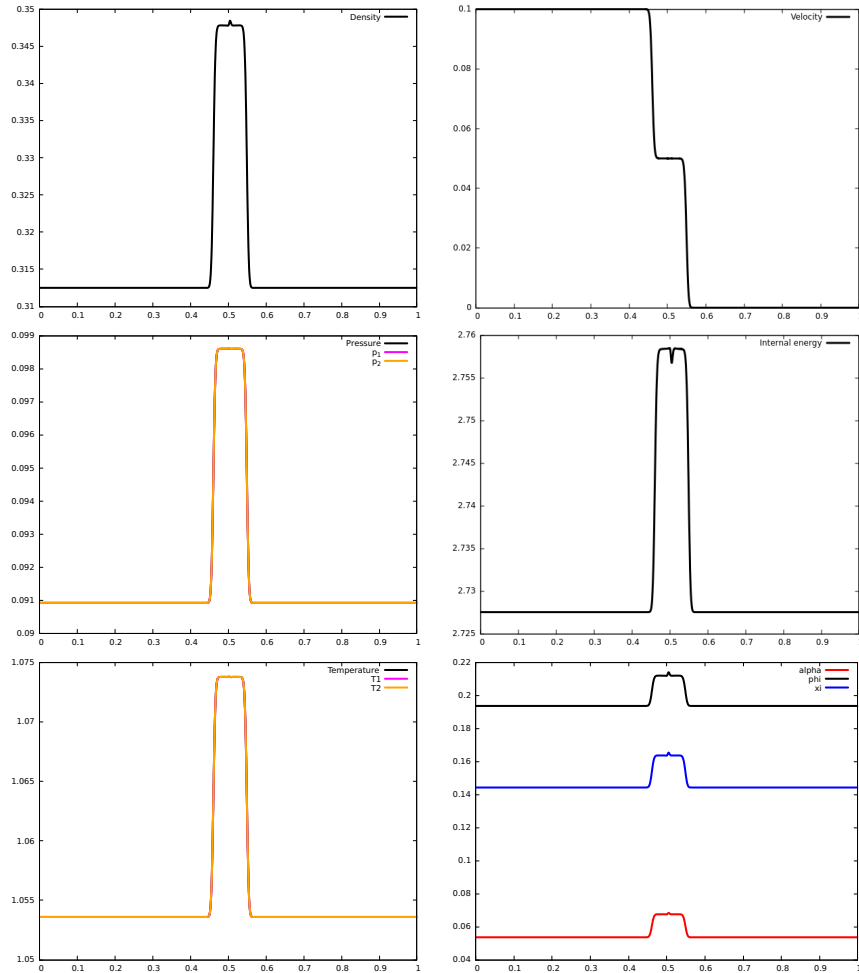


FIGURE 17. Weak acoustic perturbation of a metastable vapor state. From top left to bottom right: density profile, velocity, pressure, internal energy, temperature and fractions profile with respect to the space variable.

- 1 [9] M. De Lorenzo, Ph. Lafon, and M. Pelanti. A hyperbolic phase-transition model with non-
2 instantaneous EoS-independent relaxation procedures. *J. Comput. Phys.*, 379:279–308, 2019.
- 3 [10] G. Faccanoni, S. Kokh, and G. Allaire. Modelling and simulation of liquid-vapor phase transition
4 in compressible flows based on thermodynamical equilibrium. *ESAIM Math. Model. Numer. Anal.*,
5 46(5):1029–1054, 2012.
- 6 [11] S. Fechter, C.-D. Munz, C. Rohde, and C. Zeiler. A sharp interface method for compressible
7 liquid-vapor flow with phase transition and surface tension. *J. Comput. Phys.*, 336:347–374,
8 2017.
- 9 [12] T. Gallouët, J.-M. Hérard, and N. Seguin. Some recent finite volume schemes to compute
10 Euler equations using real gas EOS. *Internat. J. Numer. Methods Fluids*, 39(12):1073–1138,
11 2002.
- 12 [13] S. Gavriluk The structure of pressure relaxation terms: the one-velocity case. *Technical
13 report, EDF*, H-I83-2014-0276-EN, 2014.
- 14 [14] H. Ghazi. *Modélisation d’écoulements compressibles avec transition de phase et prise en
15 compte des états métastables*. PhD thesis, 2018.

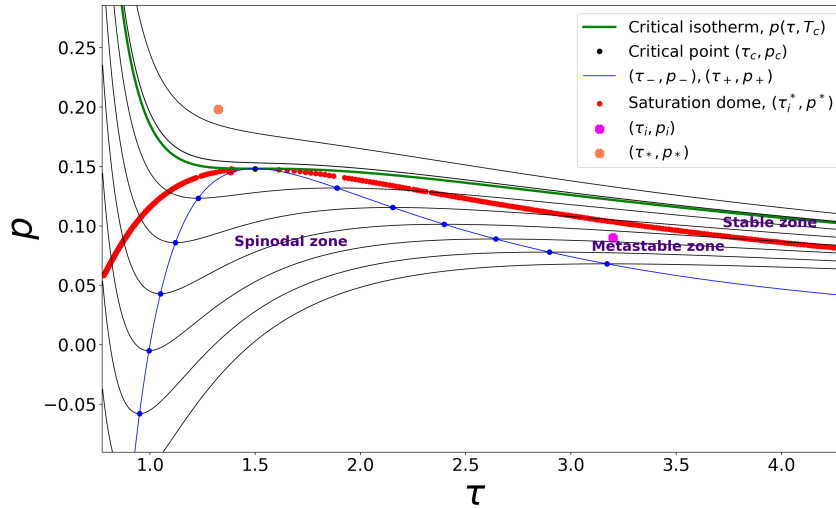


FIGURE 18. Initial (τ_i, e_i) and intermediate (τ_*, e_*) data for a strong acoustic perturbation of a metastable vapor state in plane (τ, p) .

- 1 [15] H. Ghazi, F. James, and H. Mathis. Vapour-liquid phase transition and metastability. *ESAIM: Proceedings and Surveys*, 66:22–41, 2019.
- 2
- 3 [16] J. W. Gibbs. The Collected Works of J. Willard Gibbs, vol I: Thermodynamics. *Yale University Press*, 1948.
- 4
- 5 [17] E. Godlewski, and P.A. Raviart. Hyperbolic Systems of Conservation laws. *Applied Mathematical Sciences* **118**, Springer, 1996.
- 6
- 7 [18] P. Helluy, O. Hurisse, and E. Le Coupand. Verification of a two-phase flow code based on an homogeneous model. *Int. J. Finite Vol.*, EDF Special Workshop:24, 2015.
- 8
- 9 [19] P. Helluy and H. Mathis. Pressure laws and fast Legendre transform. *Math. Models Methods Appl. Sci.*, 21(4):745–775, 2011.
- 10
- 11 [20] J.-B. Hiriart-Urruty and C. Lemaréchal. Fundamentals of convex analysis. *Grundlehren Text Editions. Springer-Verlag*, Berlin, 2001.
- 12
- 13 [21] O. Hurisse. Application of an homogeneous model to simulate the heating of two-phase flows. *Int. J. Finite Vol.*, 11:37, 2014.
- 14
- 15 [22] [10.1016/j.compfluid.2017.04.007] O. Hurisse. Numerical simulations of steady and unsteady two-phase flows using a homogeneous model. *Comput. & Fluids*, 152:88–103, 2017.
- 16
- 17 [23] O. Hurisse and L. Quibel. A homogeneous model for compressible three-phase flows involving heat and mass transfer. *ESAIM: Proceedings and Surveys*, 2019.
- 18
- 19 [24] F. James and H. Mathis. A relaxation model for liquid-vapor phase change with metastability. *Commun. Math. Sci.*, 14(8):2179–2214, 2016.
- 20
- 21 [25] A.K. Kapila, R. Menikoff, J.B. Bdzil, S.F. Son and D.S. Stewart Two-phase modelling of DDT in granular materials: reduced equations. *Phys. Fluids*, 13:3002–3024, 2001.
- 22
- 23 [26] L. D. Landau and E. M. Lifshitz, Statistical Physics: V. 5. Course of Theoretical Physics. *Pergamon press*, 1969.
- 24
- 25 [27] B. J. Lee, E. F. Toro, C. E. Castro, and N. Nikiforakis, Adaptive Osher-type scheme for the Euler equations with highly nonlinear equations of state. *J. Comput. Phys.*, 246:165–183, 2013.
- 26
- 27
- 28 [28] R. G. Mortimer. Physical Chemistry. *Academic Press Elsevier*, 2008.
- 29 [29] D.Y. Peng and D.B. Robinson. A new Two-Constant Equation of State. *Industrial and Engineering Chemistry: Fundamentals*, vol 15, 1976, p. 59-64.
- 30

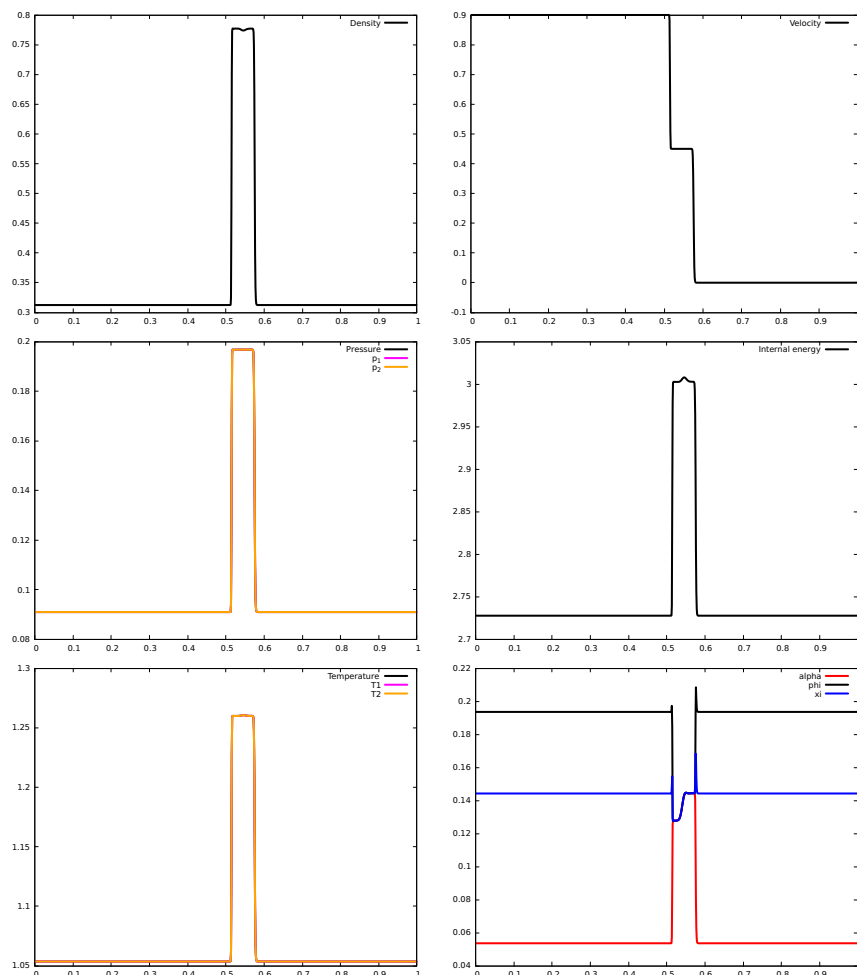


FIGURE 19. Strong acoustic perturbation of a metastable vapor state with a compression with velocity 0.9. From top left to bottom right: density profile, velocity, pressure, internal energy, temperature and fractions profile with respect to the space variable.

- 1 [30] R. T. Rockafellar. Convex analysis. *Princeton Landmarks in Mathematics. Princeton Uni-*
2 *versity Press, Princeton, NJ*, 1997. Reprint of the 1970 original, Princeton Paperbacks.
- 3 [31] R. Saurel, F. Petitpas, and R. Abgrall. Modelling phase transition in metastable liquids:
4 application to cavitating and flashing flows. *J.Fluid Mech.*, **607** (2008), 313-350.
- 5 [32] N. Shamsundarl and J.H. Lienhard. Equations of state and spinodal lines – A review. *Nuclear*
6 *engineering and design*, 141, 269–287, 1993.
- 7 [33] G. Soave. Equilibrium constants from a modified Redlich-Kwong equation of state. *Chemical*
8 *engineering science*, vol 27, 6, 1197–1203, 1972, Pergamon.
- 9 [34] E. F. Toro. Riemann solvers and numerical methods for fluid dynamics: a practical introduc-
10 tion. *Springer-Verlag, Berlin*, third edition, 2009.
- 11 [35] A. Zein, M. Hantke, and G. Warnecke, Modeling phase transition for compressible two-phase
12 flows applied to metastable liquids. *J. Comp. Phys.*, **229** (2010), 1964-2998.

- 1 (Hala Ghazi) LABORATOIRE JEAN LERAY, UNIVERSITÉ DE NANTES & CNRS UMR 6629, BP
2 92208, F-44322 NANTES CEDEX 3, FRANCE
3 *Email address:* `hala.ghazi@univ-nantes.fr`
- 4 (François James) INSTITUT DENIS POISSON, UNIVERSITÉ D'ORLÉANS & CNRS UMR 7013, BP
5 6759, F-45067 ORLÉANS CEDEX 2, FRANCE
6 *Email address:* `francois.james@univ-orleans.fr`
- 7 (Hélène Mathis) LABORATOIRE JEAN LERAY, UNIVERSITÉ DE NANTES & CNRS UMR 6629, BP
8 92208, F-44322 NANTES CEDEX 3, FRANCE
9 *Email address:* `helene.mathis@univ-nantes.fr`